An a posteriori-based, fully adaptive algorithm with adaptive stopping criteria and mesh refinement for thermal multiphasecompositional flows in porous media

Daniele Antonio Di Pietro, Martin Vohralík, Soleiman Yousef

An a posteriori-based, fully adaptive algorithm with adaptive stopping criteria and mesh refinement for thermal multiphase compositional flows in porous media*

Daniele A. Di Pietro[†1], Martin Vohralík[‡2], and Soleiman Yousef[§3,4]

[1] University of Montpellier 2, I3M, 34057 Montpellier 5, France
[2] INRIA Paris-Rocquencourt, B.P. 105, 78153 Le Chesnay, France
[3] IFP Energies nouvelles, 1 & 4 av. Bois Préau, 92852 Rueil-Malmaison, France
[4] UPMC Univ. Paris 06, UMR 7598, Laboratoire Jacques-Louis Lions, 75005, Paris, France
& CNRS, UMR 7598, Laboratoire Jacques-Louis Lions, 75005, Paris, France

December 5, 2014

Abstract

In this work we develop an a posteriori-based adaptive algorithm for thermal multiphase compositional flows in porous media. The key ingredient are fully computable a posteriori error estimates, bounding the dual norm of the residual supplemented by a nonconformity evaluation term. The theory hinges on assumptions that allow the application to variety of discretization methods. The estimators are then elaborated to estimate separately the space, time, linearization, and algebraic errors. This additional information is used to formulate a fully adaptive algorithm including adaptive stopping criteria for iterative solvers as well as refinement/derefinement criteria for both the time step and the mesh size. Numerical validation is provided on an industrial case study in the context of oil-recovery based on the steam-assisted gravity drainage procedure. Implicit cell-centered finite volumes with phase-upwind and two-point discretization of the diffusive fluxes are considered. It is shown that significant gains in computational cost can be achieved in this example, without hindering the quality of the results as measured by quantities of engineering interest.

Key words: a posteriori error analysis, adaptive mesh refinement, adaptive stopping criteria, compositional Darcy flow, thermal flow, finite volume method

1 Introduction

The thermal multiphase compositional model in porous medium describes the flow of several fluids through a subsurface under a non-isothermal condition. The governing equations are the conservation of the amount of each component and the conservation of energy, which are partial differential equations, supplemented by algebraic equations expressing the conservation of volume, the conservation of the quantity of matter, and the thermodynamic equilibrium, see [18, 19, 14].

Thermal models are especially important for simulation of the enhanced oil recovery, where the increase of temperature reduces the oil viscosity which in turn improves mobility and makes the production easier, therefore leading to better recovery indices. Several recent works deal with the simulation of thermal oil-recovery, like, e.g., [36, 17, 42, 40, 34, 39, 20, 37]. Thermal processes play also an important role in the modeling of geothermal reservoirs, see, e.g., [41] and the references therein.

*This research was supported by the ERT project "Enhanced oil recovery and geological sequestration of CO_2: mesh adaptivity, a posteriori error control, and other advanced techniques" (LJLL/IFPEN).

[†]daniele.di-pietro@univ-montp2.fr
[‡]martin.vohralik@inria.fr
[§]Corresponding author, yousef@ann.jussieu.fr

A mathematical structure of multiphase thermal models of flow in porous media is proposed in [48]. The authors derive and numerically solve a system of PDEs modeling multicomponent, two-phase, thermal fluid flow in porous media. For this purpose, they develop an algorithm that aims at a balance between stability and accuracy. This approach was used previously for reservoir simulation of black-oil model [9] and also for compositional models [8]. Recently, it has been proposed in [10, 37] to formulate the phase transitions as a set of local inequality constraints and use the complementarity approach.

Many numerical methods have been proposed for the discretization of the multiphase compositional model: finite differences and finite element methods in, e.g., [3, 7, 18, 52], mixed finite element methods in, e.g., [24, 13, 15, 16], finite volume methods in, e.g., [35, 38, 31, 5, 1, 4], and recently vertex-centered methods on general 3D meshes in [30]. In the simulation of oil recovery processes based on the injection of a hot fluid to reduce oil viscosity, a key point is to track the evolution of the saturation front. Since the location of the front evolves in time, adaptive mesh refinement is mandatory to make computations accessible. Algorithms for adaptive mesh refinement have been considered, cf. [32, 27, 17] for dynamic griding in thermal and isothermal models, and other recent contributions, cf. [47, 45, 40, 42, 34, 39, 43, 44].

In this work, we go one step further with the reduction of the computational cost by proposing a fully-adaptive algorithm based on a posteriori error estimates. As a matter of fact, the discretization of the thermal compositional model leads to a nonlinear, strongly coupled system of algebraic equations, whose resolution demands a significant computational effort even when the mesh is adaptively refined. The key idea is to develop a posteriori error estimators allowing to distinguish the different components of the error, and use them to formulate stopping criteria for the iterative algebraic and nonlinear solvers together with refinement/derefinement criteria for both the time step and the space mesh. The a posteriori error estimators are derived following the general ideas of [22], where they are used to formulate adaptive stopping criteria (without mesh adaptation) for the isothermal case. The main novelties of the present work with respect to [22] are

(i) the extension of the framework to the thermal case accounting for one additional equation expressing the energy balance. From a practical viewpoint, the main difficulty is that adding a dependence on temperature to the physical parameters embeds strongly nonlinear mechanisms in the model;

(ii) the application to adaptive mesh refinement in the context of a three-dimensional industrial case study. This is a significant step to assess the performance of the overall cost-reduction strategy and makes it more appealing for practitioners.

Other works which deserve being recognized at this point are [51, 12], where a rigorous a posteriori error analysis for the immiscible incompressible two-phase flow is developped under the assumption that the flow process is isothermal.

The present paper is organized as follows. Section 2 details the unknowns and the physical properties related to the general thermal multiphase compositional model and describes the governing equations that constitute the mathematical system of the model. In Section 3 we consider a discretization of the thermal model based on the two-points finite volume scheme in space and the backward Euler scheme in time. Linearization by the Newton method and algebraic resolution by an arbitrary iterative solver is also discussed. In Section 4 we postprocess the original phase pressures and temperature and we devise their $H_0^1(\Omega)$-conforming reconstructions, as well as $\mathbf{H}(\mathrm{div};\Omega)$-conforming fluxes needed in the a posteriori analysis. In Section 5 we introduce the weak formulation of the problem, define the corresponding error measure, and derive the a posteriori error estimate. Section 6 finally illustrates the numerical results on an enhanced oil recovery thermal process for heavy oil. We show results corresponding to adaptive mesh refinement strategy saving an important number of mesh cells during the simulation, without affecting the precision of the resolution.

2 The thermal multiphase compositional model

We consider the flow through a porous medium of several fluid phases, each composed of a finite number of components from a given set. Mass exchange between phases as well as thermal effects are accounted for. The precise formulation we use extends that of Eymard, Guichard, Herbin, and Masson [30] based on the original paper of Coats [19]; see also [33] and [22].

Let $\Omega \subset \mathbb{R}^d$, $d \geq 1$, denote a bounded connected polygonal domain with boundary $\partial\Omega$, and let $t_F > 0$. In petroleum-related applications, Ω typically represents a reservoir, while t_F is the simulation time. We denote by $\mathcal{P} = \{p\}$ and $\mathcal{C} = \{c\}$ respectively the set of phases and components. A synthetic description of the fluid system is given in terms of the component-phase matrix $\mathbf{M} = [m_{cp}]_{c\in\mathcal{C},\, p\in\mathcal{P}} \in \{0,1\}^{\mathcal{C},\mathcal{P}}$ such that, for all $c \in \mathcal{C}$ and all $p \in \mathcal{P}$, $m_{cp} = 1$ if the component c is contained in the phase p and 0 otherwise. Given the component-phase matrix, we can define, for all $p \in \mathcal{P}$, the set of components present in the phase p as $\mathcal{C}_p = \{c \in \mathcal{C};\ m_{cp} = 1\}$. Conversely, for each component $c \in \mathcal{C}$, the set of phases containing c is given by $\mathcal{P}_c = \{p \in \mathcal{P};\ m_{cp} = 1\}$.

2.1 Unknowns

The unknowns of the model are (i) the *reference pressure* P; (ii) the *temperature* T; (iii) the *saturations* $\boldsymbol{S} = (S_p)_{p\in\mathcal{P}}$, representing the fraction of the pore volume occupied by each phase; (iv) for all $p \in \mathcal{P}$, the *molar fractions* of the components present in p, $\boldsymbol{C}_p := (C_{p,c})_{c\in\mathcal{C}_p}$. The unknowns of the model are collected in the vector

$$\mathcal{X} := \begin{pmatrix} P \\ T \\ (S_p)_{p\in\mathcal{P}} \\ (C_{p,c})_{p\in\mathcal{P},c\in\mathcal{C}_p} \end{pmatrix}.$$

Finally, for each phase $p \in \mathcal{P}$ the (average) *phase pressure* is given by

$$P_p = P_p(P, \boldsymbol{S}) := P + P_{\mathrm{c}_p}(\boldsymbol{S}), \tag{2.1}$$

where $P_{\mathrm{c}_p}(\boldsymbol{S})$ is a *generalized capillary pressure*.

2.2 Fluid and medium properties

The porous medium is characterized by the following properties (the usual dependency on the unknowns is provided in brackets): (i) the *porosity* ϕ; (ii) the symmetric tensor $\mathbb{K}$ of *absolute permeability*; (iii) the *thermal conductivity* λ; (iv) the *rock energy* $e_{\mathrm{r}}(P_p, T, \mathbf{C}_p)$; (v) the *rock molar density* ζ_r. These properties can additionally depend on the space variable when heterogeneous media are considered, but it is assumed for the sake of simplicity that the dependence on time is only via the variables of the model. Next, each fluid phase $p \in \mathcal{P}$ is characterized by the following properties: (i) the *molar density* $\zeta_p(P_p, T, \boldsymbol{C}_p)$; (ii) the *mass density* $\rho_p(P_p, T, \boldsymbol{C}_p)$; (iii) the *viscosity* $\mu_p(P_p, T, \boldsymbol{C}_p)$; (iv) the *relative permeability* $k_{\mathrm{r},p}(\boldsymbol{S})$; (v) for all $c \in \mathcal{C}_p$, the *fugacity* $f_{c,p}(P_p, T, \boldsymbol{C}_p)$; (vi) the *phase enthalpy* $H_p(P_p, T, \boldsymbol{C}_p)$; (vii) the *phase internal energy* $e_p(P_p, T, \boldsymbol{C}_p)$. It is also convenient to define for each phase $p \in \mathcal{P}$ the *mobility* given by $\nu_p(P_p, T, \boldsymbol{S}, \boldsymbol{C}_p) := \zeta_p(P_p, T, \boldsymbol{C}_p)\frac{k_{\mathrm{r},p}(\boldsymbol{S})}{\mu_p(P_p,T,\boldsymbol{C}_p)}$.

2.3 The thermal multiphase compositional model

We summarize in this section the equations that govern the non-isothermal multiphase compositional flow. For each component $c \in \mathcal{C}$, we let l_c denote the *amount* (in moles) *of component* c per unit volume given by

$$l_c = l_c(\mathcal{X}) = \phi \sum_{p\in\mathcal{P}_c} \zeta_p(P_p, T, \boldsymbol{C}_p) S_p C_{p,c}. \tag{2.2}$$

The *conservation of the amount of each component* is expressed by the following system of PDEs:

$$\partial_t l_c + \nabla\cdot\boldsymbol{\Phi}_c = q_c, \qquad \forall c \in \mathcal{C}, \tag{2.3}$$

where, for each $c \in \mathcal{C}$, $q_c \in L^2((0, t_{\mathrm{F}}); L^2(\Omega))$ denotes a *source* or *sink* and the *component flux* $\boldsymbol{\Phi}_c$ has the following expression:

$$\boldsymbol{\Phi}_c := \sum_{p\in\mathcal{P}_c} \boldsymbol{\Phi}_{p,c}, \qquad \boldsymbol{\Phi}_{p,c} = \boldsymbol{\Phi}_{p,c}(P_p, T, \boldsymbol{S}, \boldsymbol{C}_p) := \nu_p(P_p, T, \boldsymbol{S}, \boldsymbol{C}_p) C_{p,c} \boldsymbol{v}_p(P_p, T, \boldsymbol{C}_p), \tag{2.4}$$

with $\boldsymbol{v}_p$ denoting the *average phase velocity* given by Darcy's law (in the following, $\boldsymbol{g}$ denotes the gravity vector acting along $-z$ and g its Euclidian norm),

$$\boldsymbol{v}_p = \boldsymbol{v}_p(P_p, T, \boldsymbol{C}_p) := -\mathbb{K}\left(\nabla P_p - \rho_p(P_p, T, \boldsymbol{C}_p)\boldsymbol{g}\right) = -\mathbb{K}\left(\nabla P_p + \rho_p(P_p, T, \boldsymbol{C}_p) g \nabla z\right). \tag{2.5}$$

The *molar energy* per unit volume is given by

$$e_H = e_H(\mathcal{X}) = \phi \sum_{p\in\mathcal{P}} \zeta_p(P_p, T, \mathbf{C}_p) e_p(P_p, T, \mathbf{C}_p) S_p + (1-\phi)\zeta_{\mathrm{r}} e_{\mathrm{r}}(P_p, T, \mathbf{C}_p). \tag{2.6}$$

The *conservation of energy* is then expressed by the following scalar PDE:

$$\partial_t e_H + \nabla\cdot\boldsymbol{\Phi}_H = Q_H, \tag{2.7}$$

where $Q_H \in L^2((0,t_{\mathrm{F}}); L^2(\Omega))$ denotes a *thermal source* or *sink* and

$$\boldsymbol{\Phi}_H := \mathbf{J} + \sum_{p\in\mathcal{P}} \boldsymbol{\Phi}_{p,H}, \tag{2.8}$$

with *Fourier flux* $\mathbf{J} = \mathbf{J}(T) := -\lambda\nabla T$ and *phase enthalpy fluxes* given by

$$\boldsymbol{\Phi}_{p,H} := \nu_p(P_p, T, \boldsymbol{S}, \mathbf{C}_p) H_p(P_p, T, \mathbf{C}_p) \boldsymbol{v}_p(P_p, T, \mathbf{C}_p).$$

For the sake of simplicity, we assume *no-flow boundary conditions*,

$$\boldsymbol{\Phi}_c\cdot\boldsymbol{n}_\Omega = 0 \text{ for all } c\in\mathcal{C} \quad \text{and} \quad \boldsymbol{\Phi}_H\cdot\boldsymbol{n}_\Omega = 0 \text{ on } \partial\Omega\times(0,t_{\mathrm{F}}), \tag{2.9}$$

where $\partial\Omega$ denotes the boundary of Ω and $\boldsymbol{n}_\Omega$ its outward normal. At $t=0$ we prescribe the *initial molar energy* and the *initial amount of each component* by setting

$$e_H(\cdot,0) = e_H^0, \qquad l_c(\cdot,0) = l_c^0 \quad \forall c\in\mathcal{C}. \tag{2.10}$$

The system is closed by the algebraic equations

$$\sum_{p\in\mathcal{P}} S_p = 1, \qquad \sum_{c\in\mathcal{C}_p} C_{p,c} = 1 \quad \forall p\in\mathcal{P}, \tag{2.11}$$

and enforcing the thermodynamic equilibrium expressed by $\sum_{c\in\mathcal{C}}(N_{\mathcal{P}_c}-1) = \sum_{p\in\mathcal{P}} N_{\mathcal{C}_p} - N_{\mathcal{C}}$ inequalities of fugacities (we have used the notation $N_{\mathcal{X}}$ for the cardinality of the set $\mathcal{X}$).

To fix the ideas, we now present an example of a thermal multiphase multicomponent model which is the case considered in the numerical experiment of Section 6 below. It is the thermal Dead Oil model of a steam-assisted gravity drainage process (SAGD), a technique of steam injection designed to increase the oil mobility.

Example 1 (Dead Oil model)**.** *In the Dead Oil model we have three phases: the water phase, the oil phase, and the steam phase, represented respectively by lowercase indices (*$\mathrm{w},\mathrm{o},\mathrm{s}$*). We use also the uppercase indices (*W,O*) to represent the two components of the model: water and oil, respectively. The system of governing equations consists of the mass conservation equation of the water component*

$$\partial_t\big(\phi(\zeta_{\mathrm{w}}S_{\mathrm{w}} + \zeta_{\mathrm{s}}S_{\mathrm{s}})\big) + \nabla\cdot(\nu_{\mathrm{w}}\boldsymbol{v}_{\mathrm{w}} + \nu_{\mathrm{s}}\boldsymbol{v}_{\mathrm{s}}) = q_{\mathrm{W}},$$

of the mass conservation equation of the oil component

$$\partial_t(\phi\zeta_{\mathrm{o}}S_{\mathrm{o}}) + \nabla\cdot(\nu_{\mathrm{o}}\boldsymbol{v}_{\mathrm{o}}) = q_{\mathrm{O}},$$

and of the energy conservation equation

$$\partial_t e_H + \nabla\cdot(\boldsymbol{u} - \lambda\nabla T) = Q_H.$$

Here,

$$e_H := \phi e + (1-\phi)\zeta_r e_r, \quad e := \sum_{p\in\{\mathrm{w},\mathrm{o},\mathrm{s}\}} \zeta_p e_p S_p, \quad \boldsymbol{u} := \sum_{p\in\{\mathrm{w},\mathrm{o},\mathrm{s}\}} \nu_p H_p \boldsymbol{v}_p.$$

The algebraic closure equations are stated as follows: the volume conservation gives

$$S_{\mathrm{w}} + S_{\mathrm{o}} + S_s = 1,$$

the structure of the model together with the conservation of the quantity of matter imply

$$C_{\mathrm{w,W}} = C_{\mathrm{s,W}} = C_{\mathrm{o,O}} = 1,$$

and the thermodynamic liquid–steam equilibrium relation reads

$$S_{\mathrm{s}} S_{\mathrm{w}} (T - T_{\mathrm{sat}}(P)) = 0.$$

We consider no-flow boundary conditions prescribed for the component fluxes,

$$\begin{aligned} (\nu_{\mathrm{w}} \boldsymbol{v}_{\mathrm{w}} + \nu_{\mathrm{s}} \boldsymbol{v}_{\mathrm{s}}) \cdot \boldsymbol{n}_\Omega &= 0, \qquad \text{on } \partial\Omega \times (0, t_F), \\ (\nu_{\mathrm{o}} \boldsymbol{v}_{\mathrm{o}}) \cdot \boldsymbol{n}_\Omega &= 0, \qquad \text{on } \partial\Omega \times (0, t_F), \end{aligned}$$

and also a condition of no-flow for the total energy flux,

$$(-\lambda \nabla T + \boldsymbol{u}) \cdot \boldsymbol{n}_\Omega = 0, \qquad \text{on } \partial\Omega \times (0, t_F).$$

Finally the initial conditions are fixed as

$$\begin{aligned} e_H(\cdot, 0) &= e_H^0, \\ \phi(\zeta_{\mathrm{w}} S_{\mathrm{w}} + \zeta_{\mathrm{s}} S_{\mathrm{s}}) &= l_{\mathrm{W}}^0, \\ \phi \zeta_{\mathrm{o}} S_{\mathrm{o}} &= l_{\mathrm{O}}^0. \end{aligned}$$

3 Discretization and resolution

We consider here a discretization of the thermal multiphase compositional model of Section 2.3, which naturally extends the scheme of [22, Section 2.2] to the non-isothermal case, see also [33]. It is a standard industrial fully implicit cell-centered finite volume method and we give full details including linearization and algebraic resolution, to be as illustrative as possible. Note, however, that the a posteriori error estimates of Section 5 apply to a wide family of various different discretizations and iterative linearization and algebraic solvers.

3.1 Space-time meshes

Let $(\tau_n)_{1 \le n \le N}$ denote a sequence of positive real numbers corresponding to the discrete time steps such that $t_{\mathrm{F}} = \sum_{n=1}^N \tau_n$. We consider the discrete times $(t^n)_{0 \le n \le N}$ such that $t^0 := 0$ and, for $1 \le n \le N$, $t^n := \sum_{i=1}^n \tau_i$; then we define the time intervals $I_n := (t^{n-1}, t^n)$. For a function of time v with sufficient regularity we let $v^n := v(t^n)$, $0 \le n \le N$, and, for $1 \le n \le N$, we define the backward differencing operator

$$\partial_t^n v := \frac{1}{\tau^n}(v^n - v^{n-1}) \tag{3.1}$$

that we shall use for both scalar- and vector-valued functions.

Let $(\mathcal{M}^n)_{0 \le n \le N}$ denote a family of meshes of the space domain Ω. For every element $M \in \mathcal{M}^n$, we denote by $|M|$ its d-dimensional Lebesgue measure and by h_M its diameter. For $0 \le n \le N$, we denote by $\mathcal{E}^n$ the set of mesh faces. Boundary faces are collected in the set $\mathcal{E}^{\mathrm{b},n} := \{\sigma \in \mathcal{E}^n;\ \sigma \subset \partial\Omega\}$ and we let $\mathcal{E}^{\mathrm{i},n} := \mathcal{E}^n \setminus \mathcal{E}^{\mathrm{b},n}$. We let also $\mathcal{E}_M^{\mathrm{i},n}$ denote the faces of an element $M \in \mathcal{M}^n$ not lying on $\partial\Omega$. For an internal face $\sigma \in \mathcal{E}^{\mathrm{i},n}$ we fix an arbitrary orientation and denote the corresponding unit normal vector by $\boldsymbol{n}_\sigma$. For a boundary face $\sigma \in \mathcal{E}^{\mathrm{b},n}$, $\boldsymbol{n}_\sigma$ coincides with the exterior unit normal $\boldsymbol{n}_\Omega$ of Ω. We assume that the family $(\mathcal{M}^n)_{0 \le n \le N}$ is superadmissible in the sense of [28, Definition 3.1]. Superadmissibility requires that for all cells $M \in \mathcal{M}^n$ there exists a point $\boldsymbol{x}_M \in M$ (the *cell center*) and for all faces $\sigma \in \mathcal{E}^n$ there exists a point $\boldsymbol{x}_\sigma \in \sigma$ (the *face center*) such that, for all faces σ lying on the boundary of M, the line segment joining $\boldsymbol{x}_M$ with $\boldsymbol{x}_\sigma$ is $\mathbb{K}^{-1}$-orthogonal to σ. Common examples of super admissible meshes are Cartesian orthogonal grids (for diagonal permeability tensor $\mathbb{K}$) or matching triangular meshes that satisfy the (strict) Delaunay condition. In what follows we let, for all $M \in \mathcal{M}^n$ and all $\sigma \in \mathcal{E}_M^{\mathrm{i},n}$, $d_{M,\sigma} := \mathrm{dist}(\boldsymbol{x}_M, \boldsymbol{x}_\sigma)$ and $\mathtt{K}_M^\sigma := \mathbb{K} \cdot \boldsymbol{n}_\sigma$. We emphasize here that superadmissibility is not needed to derive the a posteriori error estimates of Section 5 but is only needed to ensure the consistency of the two-point finite volume discretization detailed next.

3.2 Two-point finite volume discretization

In the context of two-point finite volume methods, the unknowns of the model are discretized using one value per cell: For all $0 \le n \le N$ we let

$$\mathcal{X}_{\mathcal{M}}^n := (\mathcal{X}_M^n)_{M\in\mathcal{M}^n}, \qquad \mathcal{X}_M^n := \begin{pmatrix} P_M^n \\ T_M^n \\ (S_{p,M}^n)_{p\in\mathcal{P}} \\ (C_{p,c,M}^n)_{p\in\mathcal{P},c\in\mathcal{C}_p} \end{pmatrix} \quad \forall M \in \mathcal{M}^n.$$

For all time steps $0 \le n \le N$ and all $M \in \mathcal{M}^n$, the discrete phase saturations are collected in the vector $\boldsymbol{S}_M^n := (S_{p,M}^n)_{p\in\mathcal{P}}$ while, for all $p \in \mathcal{P}$, the discrete molar fractions are collected in the vector $\boldsymbol{C}_{p,M}^n := (C_{p,c,M}^n)_{c\in\mathcal{C}_p}$. The initial condition (2.10) is augmented to

$$\mathcal{X}_{\mathcal{M}}(\cdot,0) = \mathcal{X}_{\mathcal{M}}^0, \tag{3.2}$$

with $\mathcal{X}_{\mathcal{M}}^0$ resulting from a steady-state equilibrium computation. For each phase $p \in \mathcal{P}$, the corresponding phase pressure inside each cell $M \in \mathcal{M}^n$ at time step $0 \le n \le N$ is given by

$$P_{p,M}^n = P_{p,M}^n(P_M^n, \boldsymbol{S}_M^n) := P_M^n + P_{\mathrm{c}_p}(\boldsymbol{S}_M^n). \tag{3.3}$$

The PDEs (2.3) and (2.7) expressing, respectively, the conservation of the amount of each component and of energy, are discretized by requiring, for all $1 \le n \le N$ and all $M \in \mathcal{M}^n$,

$$R_{c,M}^n(\mathcal{X}_{\mathcal{M}}^n) := |M|\partial_t^n l_{c,M} + \sum_{\sigma\in\mathcal{E}_M^{\mathrm{i},n}} F_{c,M,\sigma}(\mathcal{X}_{\mathcal{M}}^n) - |M|q_{c,M}^n = 0, \qquad \forall c \in \mathcal{C}, \tag{3.4a}$$

$$R_{H,M}^n(\mathcal{X}_{\mathcal{M}}^n) := |M|\partial_t^n e_{H,M} + \sum_{\sigma\in\mathcal{E}_M^{\mathrm{i},n}} \Big(F_{H,M,\sigma}(\mathcal{X}_{\mathcal{M}}^n) + G_{M,\sigma}(\mathcal{X}_{\mathcal{M}}^n)\Big) - |M|Q_{H,M}^n = 0, \tag{3.4b}$$

where $q_{c,M}^n := \int_{I_n}\int_M q_c/(|M|\tau_n)$, $Q_{H,M}^n := \int_{I_n}\int_M Q_H/(|M|\tau_n)$, and the accumulation terms are given, for all $0 \le n \le N$, by the following discrete versions of (2.2) and (2.6), respectively: For all $M \in \mathcal{M}^n$,

$$l_{c,M}^n = l_{c,M}(\mathcal{X}_M^n) := \phi \sum_{p\in\mathcal{P}_c} \zeta_p(P_{p,M}^n, T_M^n, \boldsymbol{C}_{p,M}^n) S_{p,M}^n C_{p,c,M}^n \qquad \forall c \in \mathcal{C}, \tag{3.5a}$$

$$e_{H,M}^n = e_{H,M}(\mathcal{X}_M^n) := \phi \sum_{p\in\mathcal{P}} \zeta_p(P_{p,M}^n, T_M^n, \mathbf{C}_{p,M}^n) S_{p,M}^n e_p(P_{p,M}^n, T_M^n, \mathbf{C}_{p,M}^n) + (1-\phi)\zeta_{\mathrm{r}} e_{\mathrm{r}}(P_{p,M}^n, T_M^n, \mathbf{C}_{p,M}^n). \tag{3.5b}$$

The total flux of a generic component $c \in \mathcal{C}$ across an interface σ results from the sum of the corresponding fluxes for each phase $p \in \mathcal{P}_c$, i.e.,

$$F_{c,M,\sigma}(\mathcal{X}_{\mathcal{M}}^n) := \sum_{p\in\mathcal{P}_c} F_{p,c,M,\sigma}(\mathcal{X}_{\mathcal{M}}^n), \tag{3.6a}$$

and, similarly, the flux $F_{H,M,\sigma}$ is given by the sum of the fluxes for each phase $p \in \mathcal{P}$, i.e.,

$$F_{H,M,\sigma}(\mathcal{X}_{\mathcal{M}}^n) := \sum_{p\in\mathcal{P}} F_{p,H,M,\sigma}(\mathcal{X}_{\mathcal{M}}^n), \tag{3.6b}$$

where, for a given phase p, any $M \in \mathcal{M}^n$, and any $\sigma \in \mathcal{E}_M^{\mathrm{i},n}$ with $\sigma = \partial M \cap \partial L$,

$$F_{p,c,M,\sigma}(\mathcal{X}_{\mathcal{M}}^n) = \nu_p^{\uparrow}(\mathcal{X}_{\mathcal{M}}^n) C_{p,c,M_p^{\uparrow}}^n F_{p,M,\sigma}(\mathcal{X}_{\mathcal{M}}^n), \qquad F_{p,H,M,\sigma}(\mathcal{X}_{\mathcal{M}}^n) = \nu_p^{\uparrow}(\mathcal{X}_{\mathcal{M}}^n) H_{p,M_p^{\uparrow}}^{\uparrow} F_{p,M,\sigma}(\mathcal{X}_{\mathcal{M}}^n), \tag{3.7}$$

with phase upstream cell $M_p^{\uparrow} = M$ if $P_{p,M}^n - P_{p,L}^n \ge 0$ and L otherwise and $C_{p,c,M_p^{\uparrow}}^n$, $H_{p,M_p^{\uparrow}}^{\uparrow}$, and $\nu_p^{\uparrow}(\mathcal{X}_{\mathcal{M}}^n) := \nu_p(P_{p,M_p^{\uparrow}}^n, T_{M_p^{\uparrow}}^n, \boldsymbol{S}_{M_p^{\uparrow}}^n, \boldsymbol{C}_{p,M_p^{\uparrow}}^n)$ denoting, respectively, the upstream molar fraction, upstream

enthalpy, and upstream mobility. In (3.7), we have introduced the two-point finite volume approximation of the normal component of the average phase velocity on σ given by

$$F_{p,M,\sigma}(\mathcal{X}_{\mathcal{M}}^n) := |\sigma| \frac{\alpha_M \alpha_L}{\alpha_M + \alpha_L} \left[P_{p,M}^n - P_{p,L}^n + \rho_{p,\sigma}^n g \left(z_M - z_L \right) \right], \qquad \alpha_K := \frac{\mathtt{K}_K^\sigma}{d_{K\sigma}} \quad \forall K \in \{M, L\}, \tag{3.8}$$

where $\rho_{p,\sigma}^n$ is an interface mass density of the phase p obtained by averaging the cell values in M and L; cf. [22] for further details. Finally, for all $M \in \mathcal{M}^n$ and all $\sigma \in \mathcal{E}_M^{\mathrm{i},n}$ with $\sigma = \partial M \cap \partial L$, the discrete Fourier flux $G_{M,\sigma}$ is given by

$$G_{M,\sigma}(\mathcal{X}_{\mathcal{M}}^n) := |\sigma| \frac{\beta_M \beta_L}{\beta_M + \beta_L} (T_M^n - T_L^n), \qquad \beta_K := \frac{\lambda_K}{d_{K\sigma}} \quad \forall K \in \{M, L\}. \tag{3.9}$$

All boundary fluxes are set to zero to account for the homogeneous natural boundary condition (2.9).

To close the system, we enforce, for all $1 \le n \le N$ and all $M \in \mathcal{M}^n$,

$$\sum_{p \in \mathcal{P}} S_{p,M}^n = 1, \qquad \sum_{c \in \mathcal{C}_p} C_{p,c,M}^n = 1 \quad \forall p \in \mathcal{P}, \tag{3.10}$$

and require that the thermodynamic equilibrium expressed in terms of $\left(\sum_{p \in \mathcal{P}} N_{\mathcal{C}_p} - N_{\mathcal{C}} \right)$ equalities of fugacities is satisfied in each cell. For further details we refer to [22] and the references therein.

3.3 Linearization and algebraic resolution

The discretization method of Section 3.2 requires to solve a system of nonlinear algebraic equations at each time step, which we do using the Newton algorithm. For $1 \le n \le N$, a given Newton iteration $k \ge 1$, and $\mathcal{X}_{\mathcal{M}}^{n,k,0}$ fixed (typically, $\mathcal{X}_{\mathcal{M}}^{n,k,0} = \mathcal{X}_{\mathcal{M}}^{n,k-1}$), we consider an iterative algebraic solver which generates a sequence $(\mathcal{X}_{\mathcal{M}}^{n,k,i})_{i \ge 1}$ solving the linear system up to the residuals given, for all $M \in \mathcal{M}^n$, by

$$R_{c,M}^{n,k,i} = \frac{|M|}{\tau^n} \left(l_{c,M}(\mathcal{X}_{\mathcal{M}}^{n,k-1}) + \mathfrak{L}_{c,M}^{n,k,i} - l_{c,M}^{n-1} \right) + \sum_{\sigma \in \mathcal{E}_M^{\mathrm{i},n}} F_{c,M,\sigma}^{n,k,i} - |M| q_{c,M}^n \qquad \forall c \in \mathcal{C}, \tag{3.11a}$$

$$R_{H,M}^{n,k,i} = \frac{|M|}{\tau^n} \left(e_{H,M}(\mathcal{X}_{\mathcal{M}}^{n,k-1}) + \mathfrak{E}_M^{n,k,i} - e_{H,M}^{n-1} \right) + \sum_{\sigma \in \mathcal{E}_M^{\mathrm{i},n}} \left(F_{H,M,\sigma}^{n,k,i} + G_{M,\sigma}^{n,k,i} \right) - |M| Q_{H,M}^n, \tag{3.11b}$$

where $\mathfrak{L}_{c,M}^{n,k,i}$ and $\mathfrak{E}_M^{n,k,i}$ are linear perturbations of the mass and energy accumulation terms defined as, respectively,

$$\mathfrak{L}_{c,M}^{n,k,i} := \frac{\partial l_{c,M}}{\partial \mathcal{X}_M^n}(\mathcal{X}_M^{n,k-1})(\mathcal{X}_M^{n,k,i} - \mathcal{X}_M^{n,k-1}), \qquad \mathfrak{E}_M^{n,k,i} := \frac{\partial e_{H,M}}{\partial \mathcal{X}_M^n}(\mathcal{X}_M^{n,k-1})(\mathcal{X}_M^{n,k,i} - \mathcal{X}_M^{n,k-1}),$$

whereas the linearized fluxes $F_{c,M,\sigma}^{n,k,i}$ and $F_{H,M,\sigma}^{n,k,i}$ read

$$F_{c,M,\sigma}^{n,k,i} := \sum_{p \in \mathcal{P}_c} F_{p,c,M,\sigma}^{n,k,i}, \qquad F_{H,M,\sigma}^{n,k,i} := \sum_{p \in \mathcal{P}} F_{p,H,M,\sigma}^{n,k,i}, \tag{3.12}$$

with linearized phase fluxes

$$F_{p,c,M,\sigma}^{n,k,i} := F_{p,c,M,\sigma}(\mathcal{X}_{\mathcal{M}}^{n,k-1}) + \sum_{M' \in \mathcal{M}^n} \frac{\partial F_{p,c,M,\sigma}}{\partial \mathcal{X}_{M'}^n}(\mathcal{X}_{\mathcal{M}}^{n,k-1})(\mathcal{X}_{M'}^{n,k,i} - \mathcal{X}_{M'}^{n,k-1}),$$

$$F_{p,H,M,\sigma}^{n,k,i} := F_{p,H,M,\sigma}(\mathcal{X}_{\mathcal{M}}^{n,k-1}) + \sum_{M' \in \mathcal{M}^n} \frac{\partial F_{p,H,M,\sigma}}{\partial \mathcal{X}_{M'}^n}(\mathcal{X}_{\mathcal{M}}^{n,k-1})(\mathcal{X}_{M'}^{n,k,i} - \mathcal{X}_{M'}^{n,k-1}).$$

Finally, the linearized energy flux reads

$$G_{M,\sigma}^{n,k,i} := G_{M,\sigma}(\mathcal{X}_{\mathcal{M}}^{n,k-1}) + \sum_{M' \in \mathcal{M}^n} \frac{\partial G_{M,\sigma}}{\partial \mathcal{X}_{M'}^n}(\mathcal{X}_{\mathcal{M}}^{n,k-1})(\mathcal{X}_{M'}^{n,k,i} - \mathcal{X}_{M'}^{n,k-1}). \tag{3.13}$$

4 Approximate solution and reconstructions

The original piecewise constant finite volume phase pressures and temperatures are unsuitable for energy-type a posteriori error analysis, as, in particular, one cannot work with their elementwise gradients. In this section, we first postprocess them into higher-order polynomials. We then prepare the flux reconstructions and smoothed phase pressures and temperatures that will be necessary in the a posteriori estimators in the next section. We will employ, for each time step n, $\mathbf{H}(\mathrm{div};\Omega)$-conforming discrete fluxes belonging to the lowest-order Raviart–Thomas–Nédélec space $\mathbf{RTN}(\mathcal{M}^n)$ (see Brezzi and Fortin [11]). Recall that, for rectangular parallelepipeds meshes such as the ones used in the numerical examples of Section 6 below,

$$\begin{aligned}\mathbf{RTN}(\mathcal{M}^n) := \{&\boldsymbol{v}_h \in \mathbf{H}(\,\mathrm{div}\,;\Omega);\ \boldsymbol{v}_h|_M \in \mathbb{Q}_{1,0}(M)\times\mathbb{Q}_{0,1}(M) \text{ if } d=2,\\ &\mathbb{Q}_{1,0,0}(M)\times\mathbb{Q}_{0,1,0}(M)\times\mathbb{Q}_{0,0,1}(M) \text{ if } d=3,\quad \forall M\in\mathcal{M}^n\}\,.\end{aligned}$$

For more general meshes one can either introduce a matching simplicial submesh of $\mathcal{M}^n$ and use the simplicial version of $\mathbf{RTN}(\mathcal{M}^n)$, or use the construction proposed in [23, Appendix A].

4.1 Post-processing of the phase pressures and temperature

Let a time step $1\le n\le N$, a Newton linearization iteration $k\ge 1$, and an algebraic solver iteration $i\ge 1$ be fixed. Following [29], we define the fluxes $\mathbf{\Gamma}_{p,h}^{n,k,i}\in\mathbf{RTN}(\mathcal{M}^n)$, $p\in\mathcal{P}$, and $\mathbf{\Gamma}_{T,h}^{n,k,i}\in\mathbf{RTN}(\mathcal{M}^n)$ such that, for all $M\in\mathcal{M}^n$ and all $\sigma\in\mathcal{E}_M^{\mathrm{i},n}$,

$$(\mathbf{\Gamma}_{p,h}^{n,k,i}\cdot\boldsymbol{n}_M,1)_\sigma = F_{p,M,\sigma}(\mathcal{X}_{\mathcal{M}}^{n,k,i})\quad\forall p\in\mathcal{P},\qquad (\mathbf{\Gamma}_{T,h}^{n,k,i}\cdot\boldsymbol{n}_M,1)_\sigma = G_{M,\sigma}(\mathcal{X}_{\mathcal{M}}^{n,k,i}),\tag{4.1}$$

with $F_{p,M,\sigma}$ and $G_{M,\sigma}$ defined by (3.8) and (3.9), respectively, and $\mathbf{\Gamma}_{p,h}^{n,k,i}\cdot\boldsymbol{n}_\Omega=0$ on $\partial\Omega$, $\mathbf{\Gamma}_{T,h}^{n,k,i}\cdot\boldsymbol{n}_\Omega=0$ on $\partial\Omega$, thereby accounting for the no flux boundary conditions (2.9). The fluxes $\mathbf{\Gamma}_{p,h}^{n,k,i}$, $p\in\mathcal{P}$, defined by (4.1) are discrete Darcy phase velocities. Motivated by the continuous constitutive relation (2.5) and following [50], we introduce for each $p\in\mathcal{P}$ the piecewise quadratic postprocessed phase pressure $P_{p,h}^{n,k,i}$ such that, for all $M\in\mathcal{M}^n$,

$$(-\mathbb{K}\nabla P_{p,h}^{n,k,i})|_M = (\mathbf{\Gamma}_{p,h}^{n,k,i})|_M - (\mathbb{K}\rho_p(P_{p,M}^{n,k,i},T_M^{n,k,i},\boldsymbol{C}_{p,M}^{n,k,i})\boldsymbol{g})|_M\quad\text{and}\quad\frac{(P_{p,h}^{n,k,i},1)_M}{|M|}=P_{p,M}^{n,k,i}.$$

Similarly, motivated by the continuous Fourier law $\mathbf{J}=-\lambda\nabla T$, we define the piecewise quadratic temperature postprocessing $T_h^{n,k,i}$ such that, for all $M\in\mathcal{M}^n$,

$$-\lambda\nabla T_h^{n,k,i}|_M = \mathbf{\Gamma}_{T,h}^{n,k,i}|_M\quad\text{and}\quad\frac{(T_h^{n,k,i},1)_M}{|M|}=T_M^{n,k,i}.$$

From the above postprocessings we define the space-time functions $P_{p,h\tau}^{n,k,i}$, $p\in\mathcal{P}$, and $T_{h\tau}^{n,k,i}$ assuming an affine-in-time behavior from the converged values at t^{n-1} and the (possibly non converged) values $P_h^{n,k,i}$, $p\in\mathcal{P}$, and $T_h^{n,k,i}$ at t^n. This complies with the backward Euler time stepping in (3.4a)–(3.4b) and will produce the weak time derivative for the operator (3.1). For further use we also define the vector of reconstructed phase pressures $\boldsymbol{P}_{h\tau}^{n,k,i}:=(P_{p,h\tau}^{n,k,i})_{p\in\mathcal{P}}$. Henceforth, ∇ is to be understood as the broken gradient operator on $\mathcal{M}^n$ when used for $P_{p,h\tau}^{n,k,i}$ or $T_{h\tau}^{n,k,i}$.

4.2 Saturations, molar fractions, amounts of components, and molar energy

The approximations of saturations, molar fractions, amounts of components, and molar energy obtained using the finite volume discretization detailed in Sections 3 are piecewise constant in space. They never appear behind the gradient operator and for this reason, we simply define for all $0\le n\le N$, $k\ge1$, and

$i \geq 1$, piecewise constant functions of space such that

$$\begin{aligned}
(S_{p,h}^{n,k,i})|_M &= S_{p,M}^{n,k,i} && \forall p \in \mathcal{P} \\
(C_{p,c,h}^{n,k,i})|_M &= C_{p,c,M}^{n,k,i} && \forall p \in \mathcal{P},\ \forall c \in \mathcal{C}_p, \\
(l_{c,h}^{n,k,i})|_M &= l_{c,M}^{n,k,i} := l_{c,M}(\mathcal{X}_{\mathcal{M}}^{n,k,i}) && \forall c \in \mathcal{C}, \\
(e_{H,h}^{n,k,i})|_M &= e_{H,M}^{n,k,i} := e_{H,M}(\mathcal{X}_{\mathcal{M}}^{n,k,i}),
\end{aligned}$$

with $l_{c,M}$ and $e_{H,M}$ defined by (3.5a) and (3.5b), respectively. The space–time functions $S_{p,h\tau}^{n,k,i}$, $p \in \mathcal{P}$, $C_{p,c,h\tau}^{n,k,i}$, $p \in \mathcal{P}$, $c \in \mathcal{C}_p$, $l_{c,h\tau}^{n,k,i}$, $c \in \mathcal{C}$, and $e_{H,h\tau}^{n,k,i}$ are then defined therefrom while being continuous and piecewise affine in time as for the pressures and temperature.

Remark 4.1. *As detailed in [22, Section 4.2.2], the relations* (3.3), (3.5a), *and* (3.5b) *may not hold precisely for the discrete approximations* $P_{h\tau}^{n,k,i}$, $T_{h\tau}^{n,k,i}$, $S_{p,h\tau}^{n,k,i}$, $C_{p,c,h\tau}^{n,k,i}$, $P_{p,h\tau}^{n,k,i}$, $e_{H,h\tau}^{n,k,i}$, *and* $l_{c,h\tau}^{n,k,i}$ *(the capillary pressure function applied to a piecewise polynomial is typically no more a piecewise polynomial and a product of two piecewise affine-in-time functions is a piecewise quadratic-in-time function). Similarly, whereas the algebraic closure equations* (3.10) *hold precisely, the equality of fugacities will be violated if the local fugacity equations are not resolved exactly. We suppose the error from all these non-satisfactions as negligible.*

4.3 H_0^1-conforming phase pressures and temperature reconstructions

The approximations defined in Section 4.1 have sufficient regularity for the application of the piecewise gradient operator, but are nonconforming. In order to define our a posteriori estimators below, following [21, 6] in the model cases, we introduce space-continuous phase pressures and temperature reconstructions defined by $\mathfrak{P}_{p,h}^{n,k,i} = \mathcal{I}_{\rm av}(P_{p,h}^{n,k,i})$ and $\mathfrak{T}_{h\tau}^{n,k,i} = \mathcal{I}_{\rm av}(T_{h\tau}^{n,k,i})$. Here $\mathcal{I}_{\rm av}$ denotes a vertex-averaging interpolator, cf., e.g., [2], simply smoothing a discontinuous piecewise polynomial to a continuous one.

4.4 $\mathbf{H}(\mathrm{div};\Omega)$-conforming flux reconstructions

Let a time step $1 \leq n \leq N$, a Newton linearization iteration $k \geq 1$, and an algebraic solver iteration $i \geq 1$ be fixed. We define several flux reconstructions for use in the a posteriori estimates of Section 5. Remark 5.2 below gives a mathematical motivation for $\mathbf{H}(\mathrm{div},\Omega))$-conforming total flux reconstructions in the present setting, whereas the estimators in Section 5.3 are based on the identification of the different error components with corresponding fluxes following [26]:

- The *discretization fluxes* $\mathbf{\Theta}_{\mathrm{dis},c,h}^{n,k,i} \in \mathbf{RTN}(\mathcal{M}^n)$, $c \in \mathcal{C}$, and $\mathbf{\Theta}_{\mathrm{dis},H,h}^{n,k,i} \in \mathbf{RTN}(\mathcal{M}^n)$ such that, for all $M \in \mathcal{M}^n$ and all $\sigma \in \mathcal{E}_M^{\mathrm{i},n}$,

$$(\mathbf{\Theta}_{\mathrm{dis},c,h}^{n,k,i}\cdot\boldsymbol{n}_M,1)_\sigma := F_{c,M,\sigma}(\mathcal{X}_{\mathcal{M}}^{n,k,i}), \qquad (\mathbf{\Theta}_{\mathrm{dis},H,h}^{n,k,i}\cdot\boldsymbol{n}_M,1)_\sigma := F_{H,M,\sigma}(\mathcal{X}_{\mathcal{M}}^{n,k,i}) + G_{M,\sigma}(\mathcal{X}_{\mathcal{M}}^{n,k,i}), \tag{4.2a}$$

  with $F_{c,M,\sigma}$, $F_{H,M,\sigma}$, and $G_{M,\sigma}$ defined by (3.6a), (3.6b), and (3.9), respectively, while $\mathbf{\Theta}_{\mathrm{dis},c,h}^{n,k,i}\cdot\boldsymbol{n}_\Omega = \mathbf{\Theta}_{\mathrm{dis},H,h}^{n,k,i}\cdot\boldsymbol{n}_\Omega = 0$ on $\partial\Omega$ coherently with (2.9).

- The *linearization error fluxes* $\mathbf{\Theta}_{\mathrm{lin},c,h}^{n,k,i} \in \mathbf{RTN}(\mathcal{M}^n)$, $c \in \mathcal{C}$, and $\mathbf{\Theta}_{\mathrm{lin},H,h}^{n,k,i} \in \mathbf{RTN}(\mathcal{M}^n)$ such that, for all $M \in \mathcal{M}^n$ and all $\sigma \in \mathcal{E}_M^{\mathrm{i},n}$,

$$\begin{aligned}
(\mathbf{\Theta}_{\mathrm{lin},c,h}^{n,k,i}\cdot\boldsymbol{n}_M,1)_\sigma &:= F_{c,M,\sigma}^{n,k,i} - F_{c,M,\sigma}(\mathcal{X}_{\mathcal{M}}^{n,k,i}), \\
(\mathbf{\Theta}_{\mathrm{lin},H,h}^{n,k,i}\cdot\boldsymbol{n}_M,1)_\sigma &:= F_{H,M,\sigma}^{n,k,i} - F_{H,M,\sigma}(\mathcal{X}_{\mathcal{M}}^{n,k,i}) + G_{M,\sigma}^{n,k,i} - G_{M,\sigma}(\mathcal{X}_{\mathcal{M}}^{n,k,i}),
\end{aligned} \tag{4.2b}$$

  with $F_{c,M,\sigma}^{n,k,i}$, $F_{H,M,\sigma}^{n,k,i}$, and $G_{M,\sigma}^{n,k,i}$ defined by (3.12)–(3.13), while $\mathbf{\Theta}_{\mathrm{lin},c,h}^{n,k,i}\cdot\boldsymbol{n}_\Omega = \mathbf{\Theta}_{\mathrm{lin},H,h}^{n,k,i}\cdot\boldsymbol{n}_\Omega = 0$ on $\partial\Omega$.

- The *algebraic error fluxes* $\boldsymbol{\Theta}^{n,k,i}_{\mathrm{alg},c,h} \in \mathbf{RTN}(\mathcal{M}^n)$, $c \in \mathcal{C}$, and $\boldsymbol{\Theta}^{n,k,i}_{\mathrm{alg},H,h} \in \mathbf{RTN}(\mathcal{M}^n)$ such that, for all $M \in \mathcal{M}^n$ and for all $\sigma \in \mathcal{E}^{\mathrm{i},n}_M$,

$$(\boldsymbol{\Theta}^{n,k,i}_{\mathrm{alg},c,h}\cdot\boldsymbol{n}_M, 1)_{\partial M} := -R^{n,k,i}_{c,M}, \qquad (\boldsymbol{\Theta}^{n,k,i}_{\mathrm{alg},H,h}\cdot\boldsymbol{n}_M, 1)_{\partial M} := -R^{n,k,i}_{H,M}, \tag{4.2c}$$

  with $R^{n,k,i}_{c,M}$ and $R^{n,k,i}_{H,M}$ defined by (3.11a) and (3.11b), and with $\boldsymbol{\Theta}^{n,k,i}_{\mathrm{alg},c,h}\cdot\boldsymbol{n}_\Omega = \boldsymbol{\Theta}^{n,k,i}_{\mathrm{alg},H,h}\cdot\boldsymbol{n}_\Omega = 0$ on $\partial\Omega$, respectively.

- The *total fluxes* $\boldsymbol{\Theta}^{n,k,i}_{c,h} \in \mathbf{RTN}(\mathcal{M}^n)$, $c \in \mathcal{C}$, and $\boldsymbol{\Theta}^{n,k,i}_{H,h} \in \mathbf{RTN}(\mathcal{M}^n)$ are then obtained from the above quantities letting

$$\boldsymbol{\Theta}^{n,k,i}_{c,h} := \boldsymbol{\Theta}^{n,k,i}_{\mathrm{dis},c,h} + \boldsymbol{\Theta}^{n,k,i}_{\mathrm{lin},c,h} + \boldsymbol{\Theta}^{n,k,i}_{\mathrm{alg},c,h}, \qquad \boldsymbol{\Theta}^{n,k,i}_{H,h} := \boldsymbol{\Theta}^{n,k,i}_{\mathrm{dis},H,h} + \boldsymbol{\Theta}^{n,k,i}_{\mathrm{lin},H,h} + \boldsymbol{\Theta}^{n,k,i}_{\mathrm{alg},H,h}. \tag{4.2d}$$

5 A posteriori error estimate

In this section we describe the weak solution for the thermal multiphase compositional model of Section 2.3, we define an error measure composed of the dual norm of the residual augmented by a nonconformity evaluation term, and derive an a posteriori estimate allowing to distinguish the different sources of the error.

5.1 Weak solution

We proceed in the same spirit as for the isothermal case considered in [22]. In the following, $(\cdot,\cdot)_D$ stands for the L^2-scalar product on $D \subset \Omega$ and $\|\cdot\|_D$ for the associated norm; the same notation is used for both scalar and vector arguments, and the subscript is dropped whenever $D = \Omega$. We define

$$X := L^2((0,t_\mathrm{F}); H^1(\Omega)), \qquad Y := H^1((0,t_\mathrm{F}); L^2(\Omega)). \tag{5.1}$$

Let $\varepsilon > 0$ be a (small) parameter which only needs to satisfy $\varepsilon \le 1$. We equip the space X with the following norm:

$$\|\varphi\|_X := \left\{\sum_{n=1}^{N}\int_{I_n}\sum_{M\in\mathcal{M}^n}\|\varphi\|^2_{X,M}\,\mathrm{d}t\right\}^{\frac12}, \qquad \|\varphi\|^2_{X,M} := \varepsilon h_M^{-2}\|\varphi\|^2_M + \|\nabla\varphi\|^2_M. \tag{5.2}$$

This choice is motivated by the homogeneous Neumann boundary conditions (2.9). Taking $\varepsilon = 0$ is possible and classical when Dirichlet (pressure and temperature) boundary conditions are prescribed at least on a part of the boundary, cf. [25, 51, 12]. We suppose sufficient regularity to satisfy:

Assumption 5.1 (Regularity of the exact solution)**.** *The weak solution of the multiphase compositional thermal problem of Section 2.3 can be characterized as follows:*

$$l_c \in Y \qquad \forall c \in \mathcal{C}, \tag{5.3a}$$
$$e_H \in Y, \tag{5.3b}$$
$$P_p(P,\boldsymbol{S}) \in X \qquad \forall p \in \mathcal{P}, \tag{5.3c}$$
$$T \in X, \tag{5.3d}$$
$$\boldsymbol{\Phi}_c \in [L^2((0,t_\mathrm{F}); L^2(\Omega))]^d \qquad \forall c \in \mathcal{C}, \tag{5.3e}$$
$$\boldsymbol{\Phi}_H \in [L^2((0,t_\mathrm{F}); L^2(\Omega))]^d, \tag{5.3f}$$
$$\int_0^{t_\mathrm{F}}\{(\partial_t l_c,\varphi)(t) - (\boldsymbol{\Phi}_c,\nabla\varphi)(t)\}\,\mathrm{d}t = \int_0^{t_\mathrm{F}}(q_c,\varphi)(t)\mathrm{d}t \qquad \forall\varphi\in X,\ \forall c\in\mathcal{C}, \tag{5.3g}$$
$$\int_0^{t_F}\{(\partial_t e_H,\varphi)(t) - (\boldsymbol{\Phi}_H,\nabla\varphi)(t)\}\,\mathrm{d}t = \int_0^{t_F}(Q_H,\varphi)(t)\mathrm{d}t \qquad \forall\varphi\in X, \tag{5.3h}$$
the initial condition (2.10) *holds,* (5.3i)
the algebraic closure equations (2.11) *and the inequalities of fugacities hold,* (5.3j)

where P_p, l_c, e_H, $\boldsymbol{\Phi}_c$, and $\boldsymbol{\Phi}_H$ are defined, respectively, by (2.1), (2.2), (2.6), (2.4), *and* (2.8).

We mention that existence and uniqueness of a weak solution has to our knowledge not been established for the general thermal multiphase compositional model. However, the following easily follows from Assumption 5.1, and simultaneously links this mathematical formulation to the physical laws behind and motivates our a posteriori error analysis with the flux reconstructions of Section 4.4.

Remark 5.2 (PDEs fluxes)**.** *It follows from* (5.3a)–(5.3b)*, the assumptions* $q_c \in L^2((0,t_\mathrm{F});\, L^2(\Omega))$*,* $Q_H \in L^2((0,t_\mathrm{F});\, L^2(\Omega))$*,* (5.3e)–(5.3f)*, and* (5.3g)–(5.3h) *that actually*

$$\begin{aligned}
&\boldsymbol{\Phi}_c, \boldsymbol{\Phi}_H \in L^2((0,t_\mathrm{F}); \mathbf{H}(\mathrm{div},\Omega)),\\
&\nabla\cdot\boldsymbol{\Phi}_c = q_c - \partial_t l_c && \forall c \in \mathcal{C},\\
&\nabla\cdot\boldsymbol{\Phi}_H = Q_H - \partial_t e_H,\\
&\boldsymbol{\Phi}_c\cdot\boldsymbol{n}_\Omega = 0 \quad \text{on } \partial\Omega\times(0,t_\mathrm{F}) && \forall c \in \mathcal{C},\\
&\boldsymbol{\Phi}_H\cdot\boldsymbol{n}_\Omega = 0 \quad \text{on } \partial\Omega\times(0,t_\mathrm{F}).
\end{aligned}$$

Thus, the component fluxes $\boldsymbol{\Phi}_H, \boldsymbol{\Phi}_c$ *have continuous normal trace in a proper weak sense, the governing equations* (2.3) *and* (2.7) *are satisfied with a weak divergence, and the boundary conditions* (2.9) *hold in the normal trace sense.*

5.2 Error measure

Consider the approximate solution as specified in Sections 4.1–4.2, defined on the whole space–time slab $\Omega\times(0,t_\mathrm{F})$ (we omit here the indices n,k,i for simplicity). We now want to evaluate its distance to a weak solution as specified in Section 5.1. For this purpose, we will use the generalization to the present context of the concept of the energy norm from the steady linear single-phase Darcy flow, following [49], [26, 51], and the references therein. In particular, following [22, Section 3.3] for the isothermal multiphase compositional model, our error measure consists here of the quantities $\mathcal{N}_c, c\in\mathcal{C}$, and $\mathcal{N}_p, p\in\mathcal{P}$, depending on $\boldsymbol{P}_{h\tau}, T_{h\tau}, \boldsymbol{S}_{h\tau}, (\boldsymbol{C}_{p,h\tau})_{p\in\mathcal{P}}$, defined as, respectively,

$$\mathcal{N}_c := \sup_{\varphi\in X, \|\varphi\|_X=1} \int_0^{t_\mathrm{F}} \left\{(\partial_t l_c - \partial_t l_{c,h\tau}, \varphi)(t) - \left(\boldsymbol{\Phi}_c - \boldsymbol{\Phi}_{c,h\tau}, \nabla\varphi\right)(t)\right\} \mathrm{d}t, \tag{5.4}$$

with the exact component fluxes $\boldsymbol{\Phi}_c$ defined by (2.4) and $\boldsymbol{\Phi}_{c,h\tau}$ given by

$$\boldsymbol{\Phi}_{c,h\tau} := \sum_{p\in\mathcal{P}_c} \boldsymbol{\Phi}_{p,c,h\tau}, \qquad \boldsymbol{\Phi}_{p,c,h\tau} := \nu_p(P_{p,h\tau}, T_{h\tau}, \boldsymbol{S}_{h\tau}, \boldsymbol{C}_{p,h\tau}) C_{p,c,h\tau} \boldsymbol{v}_p(P_{p,h\tau}, T_{h\tau}, \boldsymbol{C}_{p,h\tau}), \tag{5.5}$$

and

$$\mathcal{N}_p := \inf_{\delta_p\in X} \left\{ \sum_{c\in\mathcal{C}_p} \int_0^{t_\mathrm{F}} \left\| \boldsymbol{\Psi}_{p,c}(P_{p,h\tau})(t) - \boldsymbol{\Psi}_{p,c}(\delta_p)(t) \right\|^2 \mathrm{d}t \right\}^{\frac{1}{2}}, \tag{5.6}$$

where, for a space–time function $\varphi \in L^2((0,t_\mathrm{F}); H^1(\mathcal{M}))$ (piecewise regular in space with respect to the partitions $\mathcal{M}^n$), we have let

$$\boldsymbol{\Psi}_{p,c}(\varphi) := \nu_p(P_{p,h\tau}, T_{h\tau}, \boldsymbol{S}_{h\tau}, \boldsymbol{C}_{p,h\tau}) C_{p,c,h\tau} \mathbb{K}\nabla\varphi. \tag{5.7}$$

$\mathcal{N}_c$ of (5.4) is the dual norm of the residual of the component balances (5.3g), whereas (5.7) evaluates a possible nonconformity of the discrete phase pressures whose continuous version satisfies (5.3c).

As we consider a non-isothermal flow, we need to add other contributions to take into account the energy equation. We define

$$\begin{aligned}
\mathcal{N}_H &= \mathcal{N}_H(\boldsymbol{P}_{h\tau}, T_{h\tau}, \boldsymbol{S}_{h\tau}, (\boldsymbol{C}_{p,h\tau})_{p\in\mathcal{P}})\\
&:= \sup_{\varphi\in X, \|\varphi\|_X=1} \int_0^{t_F} \left\{(\partial_t e_H - \partial_t e_{H,h\tau}, \varphi)(t) - (\boldsymbol{\Phi}_H - \boldsymbol{\Phi}_{H,h\tau}, \nabla\varphi)(t)\right\} \mathrm{d}t,
\end{aligned} \tag{5.8}$$

with $\boldsymbol{\Phi}_H$ defined by (2.8) and $\boldsymbol{\Phi}_{H,h\tau}$ given by

$$\boldsymbol{\Phi}_{H,h\tau} := \mathbf{J}_{h\tau}(T_{h\tau}) + \sum_{p\in\mathcal{P}} \boldsymbol{\Phi}_{p,H,h\tau}, \tag{5.9}$$

where

$$\boldsymbol{\Phi}_{p,H,h\tau} := \nu_p(P_{p,h\tau}, T_{h\tau}, \boldsymbol{S}_{h\tau}, \boldsymbol{C}_{p,h\tau}) H_p(P_{p,h\tau}, T_{h\tau}, \boldsymbol{C}_{p,h\tau}) \boldsymbol{v}_p(P_{p,h\tau}, T_{h\tau}, \boldsymbol{C}_{p,h\tau}), \tag{5.10}$$

and where for a space-time function $\varphi \in L^2((0,t_{\mathrm{F}}); H^1(\mathcal{M}))$, we have let

$$\mathbf{J}_{h\tau}(\varphi) := -\lambda \nabla \varphi. \tag{5.11}$$

Note here that the definition (5.8) is the dual norm of the residual of the weak formulation (5.3h) related to the energy equation. We supplement this term by defining a nonconformity measure for the temperature,

$$\mathcal{N}_T = \mathcal{N}_T(\boldsymbol{P}_{h\tau}, T_{h\tau}, \boldsymbol{S}_{h\tau}, (\boldsymbol{C}_{p,h\tau})_{p\in\mathcal{P}}) := \inf_{\theta \in X} \left\{ \int_0^{t_F} \left\| \mathbf{J}_{h\tau}(T_{h\tau})(t) - \mathbf{J}_{h\tau}(\theta)(t) \right\|^2 \mathrm{d}t \right\}^{\frac{1}{2}}, \tag{5.12}$$

as an equivalent of (5.3d) does not necessarily hold on the discrete level. Collecting all the previous contributions, we define the error measure for the multiphase thermal compositional model as

$$\mathcal{N}_e = \mathcal{N}_e(\boldsymbol{P}_{h\tau}, T_{h\tau}, \boldsymbol{S}_{h\tau}, (\boldsymbol{C}_{p,h\tau})_{p\in\mathcal{P}}) := \left\{ \sum_{c\in\mathcal{C}} {\mathcal{N}_c}^2 + {\mathcal{N}_H}^2 \right\}^{\frac{1}{2}} + \left\{ \sum_{p\in\mathcal{P}} {\mathcal{N}_p}^2 + {\mathcal{N}_T}^2 \right\}^{\frac{1}{2}}. \tag{5.13}$$

A time-localized version of this error measure can be obtained (now for the current n,k,i-indexed approximations) as follows: For each approximation as defined in Sections 4.1–4.2, we let

$$\mathcal{N}_e^{n,k,i} := \left\{ \sum_{c\in\mathcal{C}} \mathcal{N}_c^{n,k,i\,2} + \mathcal{N}_H^{n,k,i\,2} \right\}^{\frac{1}{2}} + \left\{ \sum_{p\in\mathcal{P}} \mathcal{N}_p^{n,k,i\,2} + \mathcal{N}_T^{n,k,i\,2} \right\}^{\frac{1}{2}}, \tag{5.14}$$

with $\mathcal{N}_c^{n,k,i}$, $c\in\mathcal{C}$, $\mathcal{N}_p^{n,k,i}$, $p\in\mathcal{P}$, $\mathcal{N}_H^{n,k,i}$, and $\mathcal{N}_T^{n,k,i}$ as in (5.4), (5.6), (5.8), and (5.12), with time integration performed on I_n instead of $(0,t_F)$. Note that the error measure for the exact solution satisfying Assumption 5.1 is zero.

5.3 An a posteriori error estimate distinguishing the space, time, linearization, and algebraic errors

In this section we propose a fully computable a posteriori estimate for the time-localized error measure (5.14), that additionally allows to distinguish the different components of the error. This information is then used to formulate adaptive stopping criteria for the iterative solvers, as well as for balancing criteria for the space and time errors.

Let $1 \le n \le N$, $k \ge 1$, $i \ge 1$, and $M \in \mathcal{M}^n$. Using the preparatory material from Section 4 and proceeding as in [22], see also the references therein, we are lead to define the following error estimators: The *spatial estimators*, evaluating the error related to the spatial mesh choice, are defined by

$$\begin{aligned}\eta_{\mathrm{sp},M,c}^{n,k,i}(t) := \min\{C_{\mathrm{P},M}, \varepsilon^{-\frac{1}{2}}\} h_M \left\| q_{c,h}^n - (\tau^n)^{-1}\big(l_{c,M}(\mathcal{X}_{\mathcal{M}}^{n,k-1}) + \mathfrak{L}_{c,M}^{n,k,i} - l_{c,M}^{n-1}\big) - \nabla\cdot\boldsymbol{\Theta}_{c,h}^{n,k,i} \right\|_M \\ + \left\| \boldsymbol{\Theta}_{\mathrm{dis},c,h}^{n,k,i} - \boldsymbol{\Phi}_{c,h\tau}^{n,k,i}(t^n) \right\|_M + \left\{ \sum_{p\in\mathcal{P}_c} \big(\eta_{\mathrm{NC},M,p,c}^{n,k,i}(t)\big)^2 \right\}^{\frac{1}{2}} \qquad t\in I_n, \end{aligned} \tag{5.15a}$$

and

$$\begin{aligned}\eta_{\mathrm{sp},M,H}^{n,k,i}(t) := \min\{C_{\mathrm{P},M}, \varepsilon^{-\frac{1}{2}}\} h_M \left\| Q_{c,h}^n - (\tau^n)^{-1}(e_{H,M}(\mathcal{X}_{\mathcal{M}}^{n,k-1}) + \mathfrak{E}_{c,M}^{n,k,i} - e_{H,M}^{n-1}) - \nabla\cdot\boldsymbol{\Theta}_{H,h}^{n,k,i} \right\|_M \\ + \left\| \boldsymbol{\Theta}_{\mathrm{dis},H,h}^{n,k,i} - \boldsymbol{\Phi}_{H,h\tau}^{n,k,i}(t^n) \right\|_M + \eta_{\mathrm{NC},M,T}^{n,k,i}(t) \qquad t\in I_n, \end{aligned} \tag{5.15b}$$

the *temporal estimators*, evaluating the error related to the size of the time step, by

$$\eta_{\mathrm{tm},M,c}^{n,k,i}(t) := \left\| \boldsymbol{\Phi}_{c,h\tau}^{n,k,i}(t^n) - \boldsymbol{\Phi}_{c,h\tau}^{n,k,i}(t) \right\|_M \qquad t\in I_n, \tag{5.15c}$$

$$\eta_{\mathrm{tm},M,H}^{n,k,i}(t) := \left\| \boldsymbol{\Phi}_{H,h\tau}^{n,k,i}(t^n) - \boldsymbol{\Phi}_{H,h\tau}^{n,k,i}(t) \right\|_M \qquad t\in I_n, \tag{5.15d}$$

the *linearization estimators*, measuring the error in the linearization of the nonlinear system (3.4a)–(3.4b), by

$$\eta_{\mathrm{lin},M,c}^{n,k,i} := \left\| \boldsymbol{\Theta}_{\mathrm{lin},c,h}^{n,k,i} \right\|_M + \varepsilon^{-\frac{1}{2}} h_M(\tau^n)^{-1} \left\| l_{c,M}\big(\mathcal{X}_{\mathcal{M}}^{n,k,i}\big) - l_{c,M}\big(\mathcal{X}_{\mathcal{M}}^{n,k-1}\big) - \mathfrak{L}_{c,M}^{n,k,i} \right\|_M, \tag{5.15e}$$

$$\eta_{\mathrm{lin},M,H}^{n,k,i} := \left\| \boldsymbol{\Theta}_{\mathrm{lin},H,h}^{n,k,i} \right\|_M + \varepsilon^{-\frac{1}{2}} h_M(\tau^n)^{-1} \left\| e_{H,M}\big(\mathcal{X}_{\mathcal{M}}^{n,k,i}\big) - e_{H,M}\big(\mathcal{X}_{\mathcal{M}}^{n,k-1}\big) - \mathfrak{E}_{c,M}^{n,k,i} \right\|_M, \tag{5.15f}$$

and the *algebraic estimators*, that quantify the error in the algebraic iterative resolution of the linear system resulting from Newton linearization, by

$$\eta_{\mathrm{alg},M,c}^{n,k,i} := \left\| \boldsymbol{\Theta}_{\mathrm{alg},c,h}^{n,k,i} \right\|_M, \tag{5.15g}$$

$$\eta_{\mathrm{alg},M,H}^{n,k,i} := \left\| \boldsymbol{\Theta}_{\mathrm{alg},H,h}^{n,k,i} \right\|_M. \tag{5.15h}$$

Global versions of these estimators are given by

$$\eta_{\mathrm{sp},c}^{n,k,i} := \left\{ 4 \int_{I_n} \sum_{M\in\mathcal{M}^n} \big(\eta_{\mathrm{sp},M,c}^{n,k,i}(t)\big)^2 \mathrm{d}t \right\}^{\frac{1}{2}}, \qquad \eta_{\mathrm{sp},H}^{n,k,i} := \left\{ 4 \int_{I_n} \sum_{M\in\mathcal{M}^n} \big(\eta_{\mathrm{sp},M,H}^{n,k,i}(t)\big)^2 \mathrm{d}t \right\}^{\frac{1}{2}}, \tag{5.16a}$$

$$\eta_{\mathrm{tm},c}^{n,k,i} := \left\{ 2 \int_{I_n} \sum_{M\in\mathcal{M}^n} \big(\eta_{\mathrm{tm},M,c}^{n,k,i}(t)\big)^2 \mathrm{d}t \right\}^{\frac{1}{2}}, \qquad \eta_{\mathrm{tm},H}^{n,k,i} := \left\{ 2 \int_{I_n} \sum_{M\in\mathcal{M}^n} \big(\eta_{\mathrm{tm},M,H}^{n,k,i}(t)\big)^2 \mathrm{d}t \right\}^{\frac{1}{2}}, \tag{5.16b}$$

$$\eta_{\mathrm{lin},c}^{n,k,i} := \left\{ 2\tau^n \sum_{M\in\mathcal{M}^n} \big(\eta_{\mathrm{lin},M,c}^{n,k,i}\big)^2 \right\}^{\frac{1}{2}}, \qquad \eta_{\mathrm{lin},H}^{n,k,i} := \left\{ 2\tau^n \sum_{M\in\mathcal{M}^n} \big(\eta_{\mathrm{lin},M,H}^{n,k,i}\big)^2 \right\}^{\frac{1}{2}}, \tag{5.16c}$$

$$\eta_{\mathrm{alg},c}^{n,k,i} := \left\{ 2\tau^n \sum_{M\in\mathcal{M}^n} \big(\eta_{\mathrm{alg},M,c}^{n,k,i}\big)^2 \right\}^{\frac{1}{2}}, \qquad \eta_{\mathrm{alg},H}^{n,k,i} := \left\{ 2\tau^n \sum_{M\in\mathcal{M}^n} \big(\eta_{\mathrm{alg},M,H}^{n,k,i}\big)^2 \right\}^{\frac{1}{2}}. \tag{5.16d}$$

The following result allows to estimate the time-localized norm $\mathcal{N}_e^n$ of (5.14), cf. [22]:

Corollary 5.3 (Distinguishing the space, time, linearization, and algebraic errors)**.** *Consider a time step $1 \le n \le N$, a Newton linearization iteration $k \ge 1$, and an algebraic solver iteration $i \ge 1$. Under Assumption 5.1 there holds, with the estimators given by* (5.16)*,*

$$\mathcal{N}_e^{n,k,i} \le \left\{ \sum_{c\in\mathcal{C}} \big(\eta_{\mathrm{sp},c}^{n,k,i} + \eta_{\mathrm{tm},c}^{n,k,i} + \eta_{\mathrm{lin},c}^{n,k,i} + \eta_{\mathrm{alg},c}^{n,k,i}\big)^2 + \big(\eta_{\mathrm{sp},H}^{n,k,i} + \eta_{\mathrm{tm},H}^{n,k,i} + \eta_{\mathrm{lin},H}^{n,k,i} + \eta_{\mathrm{alg},H}^{n,k,i}\big)^2 \right\}^{\frac{1}{2}}.$$

The goal of this distinction is that we can now, as in the isothermal case [22], propose criteria for stopping the iterative algebraic solver and the iterative linearization solver when the corresponding error components do not affect significantly the overall error. Specifically, the iterative algebraic solver is stopped as soon as

$$\begin{aligned} \eta_{\mathrm{alg},c}^{n,k,i} &\le \gamma_{\mathrm{alg}}\big(\eta_{\mathrm{sp},c}^{n,k,i} + \eta_{\mathrm{tm},c}^{n,k,i} + \eta_{\mathrm{lin},c}^{n,k,i}\big), \qquad \forall c \in \mathcal{C}, \\ \eta_{\mathrm{alg},H}^{n,k,i} &\le \gamma_{\mathrm{alg}}\big(\eta_{\mathrm{sp},H}^{n,k,i} + \eta_{\mathrm{tm},H}^{n,k,i} + \eta_{\mathrm{lin},H}^{n,k,i}\big) \end{aligned} \tag{5.17}$$

for s user-given positive parameter γ_{alg}. This condition reflects the fact that the algebraic errors should be small with respect to the other error components, but not necessarily excessively small, as it is usually the case in practice. Remark that the resulting criterion is adaptive since both the left- and the right-hand sides of (5.17) evolve during the iterations.

Similarly, the Newton solver is stopped according to the criterion

$$\begin{aligned} \eta_{\mathrm{lin},c}^{n,k,i} &\le \gamma_{\mathrm{lin}}\big(\eta_{\mathrm{sp},c}^{n,k,i} + \eta_{\mathrm{tm},c}^{n,k,i}\big), \qquad \forall c \in \mathcal{C}, \\ \eta_{\mathrm{lin},H}^{n,k,i} &\le \gamma_{\mathrm{lin}}\big(\eta_{\mathrm{sp},H}^{n,k,i} + \eta_{\mathrm{tm},H}^{n,k,i}\big), \end{aligned} \tag{5.18}$$

whereas the time and space mesh sizes shall be chosen so as to meet the balancing criterion

$$\begin{aligned} \gamma_{\mathrm{tm}}\eta_{\mathrm{sp},c}^{n,k,i} \le \eta_{\mathrm{tm},c}^{n,k,i} \le \Gamma_{\mathrm{tm}}\eta_{\mathrm{sp},c}^{n,k,i} \qquad \forall c \in \mathcal{C}, \\ \gamma_{\mathrm{tm}}\eta_{\mathrm{sp},H}^{n,k,i} \le \eta_{\mathrm{tm},H}^{n,k,i} \le \Gamma_{\mathrm{tm}}\eta_{\mathrm{sp},H}^{n,k,i}. \end{aligned} \tag{5.19}$$

Again, γ_{lin}, γ_{tm}, and Γ_{tm} are user-given weighting parameters (typically of order 0.1).

6 Test case

In this Section we present an SAGD process simulation, precisely the Dead Oil model of Example 1. The discretization is as described in Section 3, and the error is controlled via the a posteriori error estimate of Corollary 5.3. More precisely, we focus on space–time adaptivity, in opposition to [22], where the meshes were fixed and the emphasis was on the computational gains possible via the adaptive stopping criteria (5.17)–(5.18).

6.1 Model description

The reservoir considered in this test case is a 3-dimensional parallelepiped (100m $\times$ 1400m $\times$ 55m) discretized by a nonuniform Cartesian grid, see Figure 1, right. We consider a homogeneous anisotropic reservoir with 35% porosity, $1.94 \cdot 10^{-12}$ m^2 horizontal permeability, and $0.97 \cdot 10^{-12}$ m^2 vertical permeability. Two horizontal wells, injection and production, (in the Y direction) perforate the reservoir, see Figure 1, left.

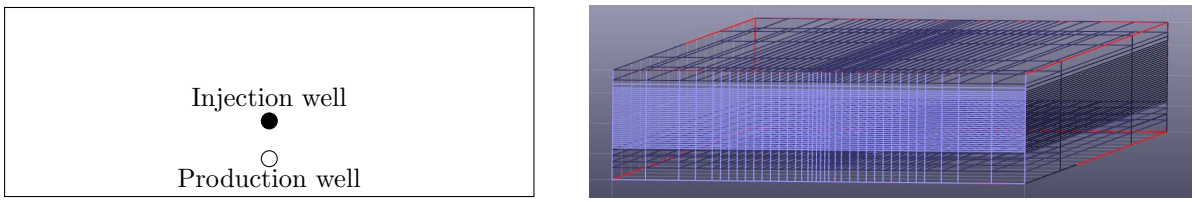

Figure 1: Reservoir mesh

The fluid is a heavy, viscous oil. Viscosity range is tabulated as a function of temperature, from $1.68 \cdot 10^3$Pa·s (at 23.89°C) to $0.741 \cdot 10^{-3}$Pa·s (at 455.44°C). The initial water saturation is equal to 0.15, so that the initial oil saturation is equal to 0.85. The mass density of the oil for this test case is given by the formula

$$\rho_{\mathrm{o}}(P,T) = \rho_{\mathrm{o,O}}(P,T) = \rho_{\mathrm{o}}^{\mathrm{ref}}\big[1 + c_{\mathrm{O}}(P - P^{\mathrm{ref}}) + d_{\mathrm{O}}(T - T^{\mathrm{ref}})\big],$$

with a constant compressibility of the oil component $c_{\mathrm{O}} = 72.5 \cdot 10^{-11}\mathrm{Pa}^{-1}$, a constant thermal expansion of the oil component $d_{\mathrm{O}} = 8.5 \cdot 10^{-4}\mathrm{K}^{-1}$, and a constant reference mass density $\rho_o^{\mathrm{ref}} = 63.304$. The water mass density is given by

$$\rho_{\mathrm{w}}(T) = \alpha_1 + \alpha_2 T + \alpha_3 T^2,$$

with $\alpha_1 = 7.81 \cdot 10^2, \alpha_2 = 1.63 \cdot 10^0$, and $\alpha_3 = -3.06 \cdot 10^{-3}$. Water viscosity is given following [46] by $1.002 \cdot 10^{-3}$Pa·s at 20°C.

The capillary pressure is set to zero and the relative permeability is shown in Figure 2. The thermal conductivity $\lambda(t)$ of the rock is constant equal to $4.76\mathrm{W} \cdot \mathrm{m}^{-1} \cdot \mathrm{K}^{-1}$. We mention that the thermal properties of the rock are those of the so-called saturated rock. The compressibility of the rock is constant equal to $43.5 \cdot 10^{-10}\mathrm{Pa}^{-1}$ and the lost in heat in the foot-wall is not simulated.

The SAGD process is simulated for $t_{\mathrm{F}} = 10$ years. The reservoir is initially assumed at hydrostatic equilibrium with a constant temperature equaling to 11°C. The initial pressure is $7.27 \cdot 10^5$Pa at -400m. To get started the production of the reservoir we begin with a heating phase of the surrounding region of production and injection wells in a period of 90 days. Then, the production well is put into production for one day with high rate of liquid flow without injection to bring down the pressure in the injection zone. Finally a period of injection/production (until 10 years) is held during the simulation. In the model, the injection and production rates are controlled by the pressure ($24.81 \cdot 10^5$Pa for the producer and $25.36 \cdot 10^5$Pa for the injector).

6.2 Approximate solution and a posteriori estimate

We show here the behavior of the approximate solution and of our a posteriori error estimates during the simulation on a fixed fine grid.

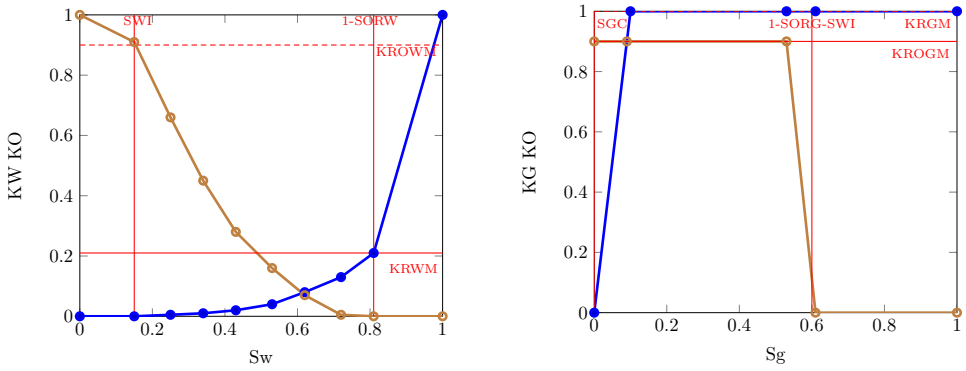

Figure 2: Relative permeability

We consider the situation where in fact the criteria (5.17) and (5.18) are satisfied with very small values of γ_{alg} and γ_{lin}, both of order 10^{-8}. This corresponds to the usual "over-resolution" but "safe-guard" reservoir practice. Also the criterion (5.19) is satisfied with $\gamma_{\text{tm}} = 0.7$ and $\Gamma_{\text{tm}} = 1.3$. Thus the estimators η^n_{sp} on themselves correctly represent not only the spatial, but also the overall error.

Figure 3 shows the evolution of the oil saturation and of the corresponding spatial estimator of the oil phase $\eta^n_{\text{sp},M,\text{o}}$ (5.15a) at different time steps. An increased error is detected around the wells, and, importantly, the estimator predicts higher error values following the movement of the oil front in the reservoir. This result suggests the use of $\eta^n_{\text{sp},M,\text{o}}$ for driving mesh adaptivity.

The results of the evolution of temperature and the temperature's spatial estimator ($\eta^n_{\text{sp},M,T}$ (5.15b)) are then summarized in Figure 4. The prediction points out an important error in the zone that follows the temperature front during the simulation, again proposing the estimator for adaptivity steering.

6.3 Adaptive mesh refinement

In this section we finally numerically assess an adaptive mesh refinement (AMR) strategy based on the space error indicators η^n_{sp}, by comparing the results with a reference solution obtained on a fine grid. As we have a symmetry in the domain, of the flow of the fluid, see Figure 3, and of the diffusion of temperature, see Figure 4, we depict the results in what follows on the half of the domain only. To refine the mesh adaptively we use a criterion based on the spatial estimator of the steam phase $\eta^n_{\text{sp},M,\text{o}}$ (5.15a). The algorithm that describes the adaptive strategy can be sketched as follows:

Algorithm 6.1 (Adaptive algorithm)**.**

Fix the fractions of cells to refine, ζ_{ref}, and to derefine, ζ_{deref}
while $t^n \leq t_{\text{F}}$ **do** {Time loop}
  Solve the system (3.4a)–(3.4b).
  Compute the spatial and temporal estimators.
  Refine the cells $M \in \mathcal{M}^n$ such that $\eta^n_{\text{sp},M,\text{o}} \geq \zeta_{\text{ref}} \max_{L\in\mathcal{M}^n} \{\eta^n_{\text{sp},L,\text{o}}\}$.
  Derefine the cells $M \in \mathcal{M}^n$ such that $\eta^n_{\text{sp},M,\text{o}} \leq \zeta_{\text{deref}} \max_{L\in\mathcal{M}^n} \{\eta^n_{\text{sp},L,\text{o}}\}$.
  Adapt the time step if (5.19) does not hold.
end while

In our industrial test case we deal with nonconforming Cartesian meshes. To compute the nonconforming flux on a parent edge, which is composed of two children edges, we first compute the flux on children edges like in the conforming case and then we gather the fluxes from the children edges to the parent one. The resulting flux is then used is in a conforming case.

Figure 5 shows the evolution of the approximate steam saturation at different simulation times while using this algorithm. We remark that the refinement follows the front of the steam saturation as time evolves, and then the derefinement process is effected in the zones abandoned by the steam front. Similar results can be appreciated in Figure 6 where we present the evolution of the temperature at several chosen time steps. A refinement that follows the diffusion of temperature can be observed, as well as a derefinement in the non-exposed zone.

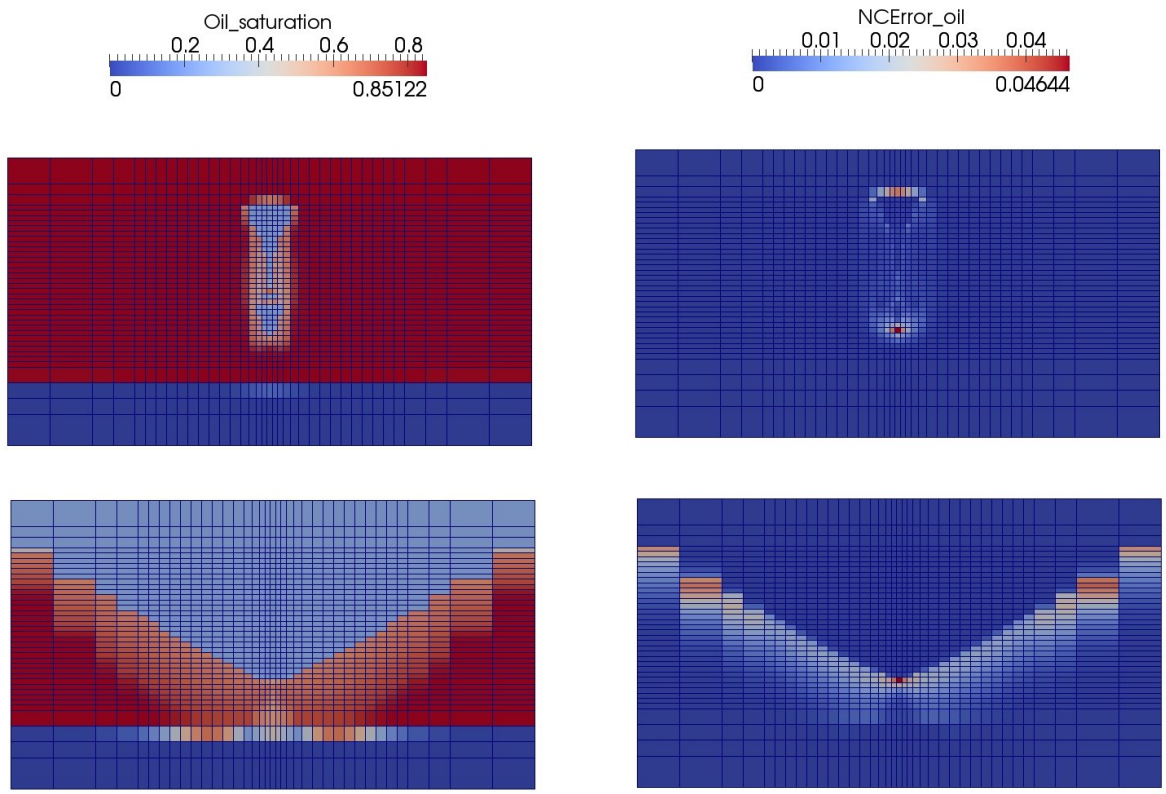

Figure 3: Approximate oil saturation (left) and spatial estimator of the oil phase (right) at 400 and 2800 days (fixed mesh)

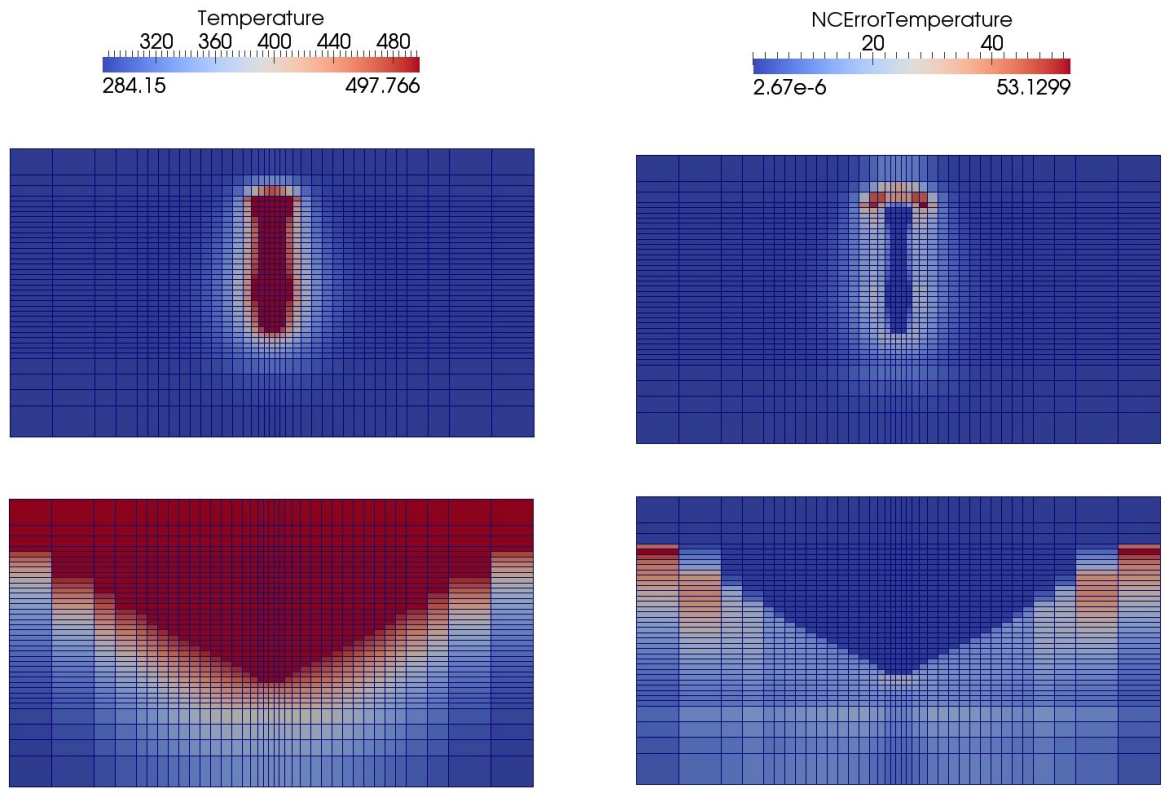

Figure 4: Approximate temperature (left) and temperature spatial estimator (right) at 400 and 2800 days (fixed mesh)

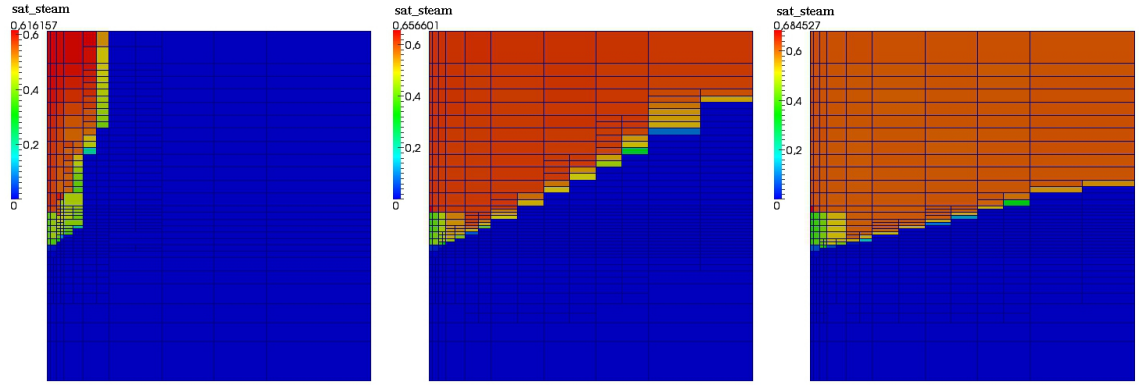

Figure 5: Approximate steam saturation at 2, 8, and 10 years (adaptively refined mesh)

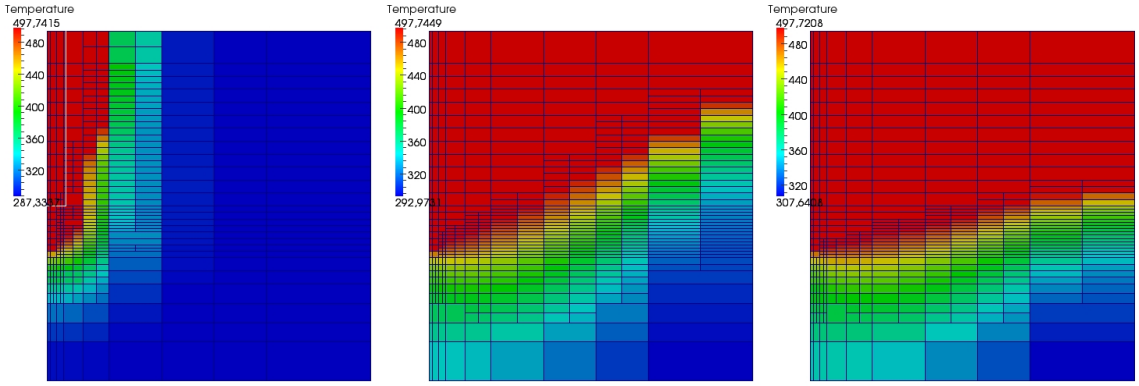

Figure 6: Approximate temperature at 2, , 8, and 10 years (adaptively refined mesh)

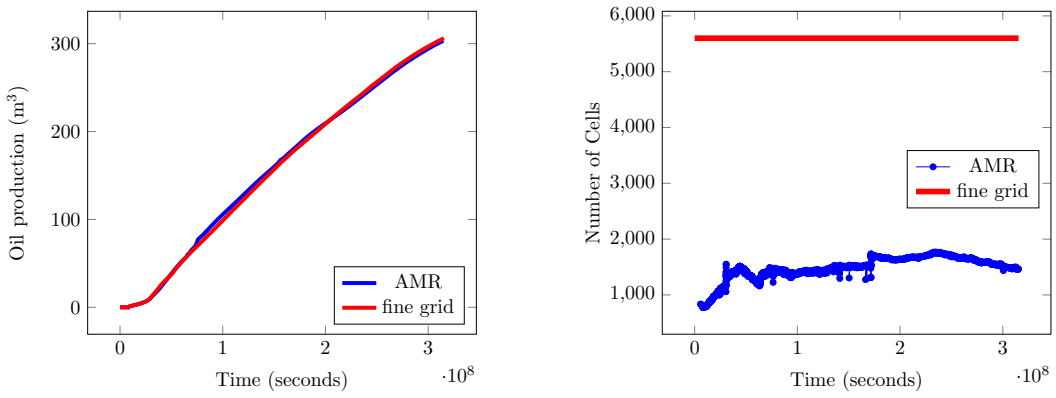

(a) Cumulative oil production as a function of time

(b) Number of cells as a function of time

Figure 7: Fine grid vs. adaptive mesh refinement. Average reduction of the number of cells : 75%.

The efficiency of the adaptive algorithm based on the spatial a posteriori estimator can be appreciated in Figure 7. Figure 7a illustrates the cumulated rate of oil production during the simulation; we compare here the result on the fine grid and the result with adaptive mesh refinement. We observe that applying the refinement strategy does not affect the accuracy of the predicted oil production, which is industrially the most important quantity. The cumulative number of cells during the simulation is then shown in Figure 7b. We remark an important reduction in terms of the number of cells using the adaptive mesh refinement strategy in comparison with the resolution on the fine grid. On average, the number of cells is reduced by 75%, which is a very important gain.

The adaptive procedure becomes still much more interesting when the adaptive stopping criteria (5.17)–(5.18) are also employed. Extensive numerical tests of [22] show that speed-ups by up to an order of magnitude are achieved on a given mesh, and this would combine with the present mesh adaptation.

References

[1] Aavatsmark, I., Barkve, T., Bøe, O., and Mannseth, T. Discretization on non-orthogonal, curvilinear grids for multi-phase flow. In *Proc. of the 4th European Conf. on the Mathematics of Oil Recovery* (Røros, Norway, 1994), vol. D.

[2] Achdou, Y., Bernardi, C., and Coquel, F. A priori and a posteriori analysis of finite volume discretizations of Darcy's equations. *Numer. Math. 96*, 1 (2003), 17–42.

[3] Acs, G., and Farkas, E. General purpose compositional model. *Society of Petroleum Engineers 25*, 4 (1985), 543–553.

[4] Agélas, L., Di Pietro, D. A., and Droniou, J. The G method for heterogeneous anisotropic diffusion on general meshes. *M2AN Math. Model. Numer. Anal. 44*, 4 (2010), 597–625.

[5] Agélas, L., Di Pietro, D. A., and Masson, R. A symmetric and coercive finite volume scheme for multiphase porous media flow problems with applications in the oil industry. In *Finite volumes for complex applications V*. ISTE, London, 2008, pp. 35–51.

[6] Ainsworth, M. Robust a posteriori error estimation for nonconforming finite element approximation. *SIAM J. Numer. Anal. 42*, 6 (2005), 2320–2341.

[7] Aziz, K., and Settari, A. *Petroleum Reservoir Simulation.* Applied Science Publisher, Ltd, London, 1979.

[8] Bell, J. B., and Trangenstein, J. Mathematical structure of compositional reservoir simulation. *SIAM J. Sci. Stat. Comput., vol. 10, pp. 817-845* (1989).

[9] Bell, J. B., and Trangenstein, J. Mathematical structure of the black-oil model for petroleum reservoir simulation. *SIAM J. Appl. Math., vol.49, pp. 749-783* (1989).

[10] Ben Gharbia, I., and Jaffré, J. Gas phase appearance and disappearance as a problem with complementarity constraints. HAL Preprint 00641621, submitted for publication, 2011.

[11] Brezzi, F., and Fortin, M. *Mixed and hybrid finite element methods*, vol. 15 of *Springer Series in Computational Mathematics*. Springer-Verlag, New York, 1991.

[12] Cancès, C., Pop, I. S., and Vohralík, M. An a posteriori error estimate for vertex-centered finite volume discretizations of immiscible incompressible two-phase flow. *Math. Comp.* (2013). DOI 10.1090/S0025-5718-2013-02723-8.

[13] Chen, Z., and Ewing, R. From single-phase to compositional flow: Applicability of mixed finite elements. *Transport in Porous Media 27* (1997), 225–242.

[14] Chen, Z., Huan, G., and Ma, Y. *Computational methods for multiphase flows in porous media.* Computational Science & Engineering. Society for Industrial and Applied Mathematics (SIAM), Philadelphia, PA, 2006.

[15] Chen, Z., Qin, G., and Ewing, R. E. Analysis of a compositional model for fluid flow in porous media. *SIAM J. Appl. Math. 60*, 3 (2000), 747–777.

[16] Chen, Z., and Yu, X. Implementation of mixed methods as finite difference methods and applications to nonisothermal multiphase flow in porous media. *Math. Comp. 24* (2006), 281–294.

[17] Christensen, J., Darche, G., Dechelette, B., Ma, H., and Sammon, P. Applications of dynamic gridding to thermal simulations. *Society of Petroleum Engineers* (16-18 March 2004).

[18] Coats, K. H. An equation of state compositional model. *Society of Petroleum Engineers 20*, 5 (1980), 363–376.

[19] Coats, K. H. Implicit compositional simulation of single porosity and dual-porosity reservoirs. *Society of Petroleum Engineers* (February 1989), 6–8.

[20] Delshad, M., Thomas, S., and Wheeler, M. Parallel numerical reservoir simulations of non-isothermal compositional flow and chemistry. *Society of Petroleum Engineers 16*, 2 (2011), 727–742.

[21] Destuynder, P., and Métivet, B. Explicit error bounds for a nonconforming finite element method. *SIAM J. Numer. Anal. 35*, 5 (1998), 2099–2115.

[22] Di Pietro, D. A., Flauraud, E., Vohralík, M., and Yousef, S. A posteriori error estimates, stopping criteria, and adaptivity for multiphase compositional Darcy flows in porous media. *J. Comput. Phys.* (2014). DOI 10.1016/j.jcp.2014.06.061.

[23] Di Pietro, D. A., and Lemaire, S. An extension of the Crouzeix–Raviart space to general meshes with application to quasi-incompressible linear elasticity and Stokes flow. *Math. Comp.* (2013). Accepted for publication.

[24] Douglas, Jr., J., Ewing, R. E., and Wheeler, M. F. The approximation of the pressure by a mixed method in the simulation of miscible displacement. *RAIRO Modél. Math. Anal. Numér. 17*, 1 (1983), 17–33.

[25] Ern, A., and Vohralík, M. A posteriori error estimation based on potential and flux reconstruction for the heat equation. *SIAM J. Numer. Anal. 48*, 1 (2010), 198–223.

[26] Ern, A., and Vohralík, M. Adaptive inexact Newton methods with a posteriori stopping criteria for nonlinear diffusion PDEs. *SIAM J. Sci. Comput. 35*, 4 (2013), A1761–A1791.

[27] Ewing, R. E., Boyett, B. A., Babu, D. K., and Heinemann, R. F. Efficient use of locally refined grids for multiphase reservoir simulation. *Society of Petroleum Engineers* (1989).

[28] Eymard, R., Gallouët, T., and Herbin, R. *The finite volume method*, vol. 7 of *Handbook of Numerical Analysis*. P. G. Ciarlet and J.-L. Lions eds., North Holland, 2000.

[29] Eymard, R., Gallouët, T., and Herbin, R. Finite volume approximation of elliptic problems and convergence of an approximate gradient. *Appl. Numer. Math. 37*, 1-2 (2001), 31–53.

[30] Eymard, R., Guichard, C., Herbin, R., and Masson, R. Vertex-centred discretization of multiphase compositional Darcy flows on general meshes. *Comput. Geosci. 16*, 4 (2012), 987–1005.

[31] Eymard, R., Herbin, R., and Michel, A. Mathematical study of a petroleum-engineering scheme. *M2AN Math. Model. Numer. Anal. 37*, 6 (2003), 937–972.

[32] Heinemann, Z. E. Using local grid refinement in a multiple-application reservoir simulator. *Society of Petroleum Engineers* (1983).

[33] Heinry, C. *Adaptive finite volume method based on a posteriori error estimators for solving two phase flow in porous media*. Ph.D. thesis, Université Pierre et Marie Curie (Paris 6), 2013.

[34] Huang, C., Yang, Y., and Deo, M. A new thermal-compositional reservoir simulator with a novel "equation line-up" method. *Society of Petroleum Engineers* (11-14 November 2007).

[35] Huber, R., and Helmig, R. Node-centered finite volume discretizations for the numerical simulation of multiphase flow in heterogeneous porous media. *Comput. Geosci. 4*, 2 (2000), 141–164.

[36] Lacroix, S., Vassilevski, Y., Wheeler, J., and Wheeler, M. Iterative solution methods for modeling multiphase flow in porous media fully implicitly. *SIAM J. Sci. Comput. 25*, 3 (2003), 905–926.

[37] Lauser, A., Hager, C., Helmig, R., and Wohlmuth, B. I. A new approach for phase transitions in miscible multi-phase flow in porous media. *Advances in Water Resources 34*, 8 (2011), 957–966.

[38] Laydi, M. R., and Ghilani, M. A general finite volume scheme for an elliptic-hyperbolic system using a variational approach. *Zeitschrift für angewandte Mathematik und Physik ZAMP 49*, 4 (1998), 630–643.

[39] Liu, K., Subramanian, G., Dratler, D., Lebel, J., and Yerian, J. A general unstructured grid, EOS-based, fully implicit thermal simulator for complex reservoir processes. *Society of Petroleum Engineers* (26-28 February 2007).

[40] Nilsson, J., Gerritsen, M., and Younis, R. An adaptive, high-resolution simulation for steam-injection processes. *Society of Petroleum Engineers* (2005).

[41] O'Sullivan, M. J., Pruess, K., and Lippmann, M. J. State of the art of geothermal reservoir simulation. *Geothermics 30*, 4 (2001), 395 – 429.

[42] Pasarai, U., and Arihara, N. A simulator for predicting thermal recovery behavior based on streamline method. *Society of Petroleum Engineers* (5-6 December 2005).

[43] Pau, G. S. H., Almgren, A. S., Bell, J. B., and Lijewski, M. J. A parallel second-order adaptive mesh algorithm for incompressible flow in porous media. *Philos. Trans. R. Soc. Lond. Ser. A Math. Phys. Eng. Sci. 367*, 1907 (2009), 4633–4654.

[44] Pau, G. S. H., Bell, J. B., Almgren, A. S., Fagnan, K. M., and Lijewski, M. J. An adaptive mesh refinement algorithm for compressible two-phase flow in porous media. *Comput. Geosci. 16*, 3 (2012), 577–592.

[45] Sammon, P. H. Dynamic grid refinement and amalgamation for compositional simulation. *Society of Petroleum Engineers* (2003).

[46] Schmidt, E. *Properties of water and steam in S.I. units.* Springer, Pennsylvania State University, 1981.

[47] Trangenstein, J. A. Multi-scale iterative techniques and adaptive mesh refinement for flow in porous media. *Advances in Water Resources 25*, 8-12 (2002), 1175 – 1213.

[48] van Odyck, D. E. A., Bell, J. B., Monmont, F., and Nikiforakis, N. The mathematical structure of multiphase thermal models of flow in porous media. *Proc. R. Soc. Lond. Ser. A Math. Phys. Eng. Sci. 465*, 2102 (2009), 523–549.

[49] Verfürth, R. Robust a posteriori error estimates for nonstationary convection-diffusion equations. *SIAM J. Numer. Anal. 43*, 4 (2005), 1783–1802.

[50] Vohralík, M. Residual flux-based a posteriori error estimates for finite volume and related locally conservative methods. *Numer. Math. 111*, 1 (2008), 121–158.

[51] Vohralík, M., and Wheeler, M. F. A posteriori error estimates, stopping criteria, and adaptivity for two-phase flows. *Comput. Geosci. 17*, 5 (2013), 789–812.

[52] Young, L. C., and Stephenson, R. E. A generalized compositional approach for reservoir simulation. *Society of Petroleum Engineers 23*, 5 (1983), 727–742.